• Original Paper •

Assessment of Wet Season Precipitation in the Central United States by the Regional Climate Simulation of the WRFG Member in NARCCAP and Its Relationship with Large-Scale Circulation Biases

Yating ZHAO[1,2], Ming XUE[*1,2], Jing JIANG[†,1], Xiao-Ming HU[2], and Anning HUANG[1]

[1]*School of Atmospheric Sciences*, *Nanjing University*, *Nanjing* 210023, *China*
[2]*Center for Analysis and Prediction of Storms and School of Meteorology*,
The University of Oklahoma, *Norman* 73072, *U.S.A*

ABSTRACT

Assessment of past-climate simulations of regional climate models (RCMs) is important for understanding the reliability of RCMs when used to project future regional climate. Here, we assess the performance and discuss possible causes of biases in a WRF-based RCM with a grid spacing of 50 km, named WRFG, from the North American Regional Climate Change Assessment Program (NARCCAP) in simulating wet season precipitation over the Central United States for a period when observational data are available. The RCM reproduces key features of the precipitation distribution characteristics during late spring to early summer, although it tends to underestimate the magnitude of precipitation. This dry bias is partially due to the model's lack of skill in simulating nocturnal precipitation related to the lack of eastward propagating convective systems in the simulation. Inaccuracy in reproducing large-scale circulation and environmental conditions is another contributing factor. The too weak simulated pressure gradient between the Rocky Mountains and the Gulf of Mexico results in weaker southerly winds in between, leading to a reduction of warm moist air transport from the Gulf to the Central Great Plains. The simulated low-level horizontal convergence fields are less favorable for upward motion than in the NARR and hence, for the development of moist convection as well. Therefore, a careful examination of an RCM's deficiencies and the identification of the source of errors are important when using the RCM to project precipitation changes in future climate scenarios.

Key words: NARCCAP, Central United States, precipitation, low-level jet, large-scale environment, diurnal variation

Article Highlights:

• The assessed climate model reproduces the key features of wet-season precipitation distribution but underestimates the amount in the Central U.S.
• The lack of eastward propagating convective systems from the Rockies into the Central Plains in simulations contributes to the dry bias
• Inaccuracies in large-scale circulation and environmental conditions from the Gulf to Great Plains also contribute to precipitation errors

---

1. Introduction

The North American Regional Climate Change Assessment Program (NARCCAP; Mearns et al., 2009) is a project that uses six regional climate models (RCMs) to produce dynamically downscaled regional climate simulations to in-vestigate the uncertainties in projecting future climate under different climate change scenarios for impact research (http://www.narccap.ucar.edu/about/index.html). These RCMs are the Canadian Regional Climate Model (CRCM) (Caya and Laprise, 1999), the Scripps Experimental Climate Prediction Center (ECPC) Regional Spectral Model (Juang et al., 1997), the Hadley Centre's regional model version 3 (HadRM3) (Pope et al., 2000), the fifth-generation Pennsylvania State University-National Center for Atmospheric Research (NCAR) Mesoscale Model (MM5) (Grell et al.,

---

* Corresponding author: Ming XUE
  Email: mxue@ou.edu
† Deceased 3 Jan 2023

1994), the Regional Climate Model version 3 (RegCM3) (Giorgi et al., 1993a, b), and the Weather Research and Forecasting model with the Grell-Devenyi cumulus scheme (WRFG) (Grell and Dévényi, 2002). In the NARCCAP program, these RCMs are used to simulate regional climate for a historical period and to downscale coupled atmosphere–ocean general circulation models forced with the A2 emission scenario (Nakicenovic et al., 2000).

To understand the potential reliability of the RCMs for future climate simulations, it is necessary to assess their simulation performance for historical periods when observational data are available (Pan et al., 2001; Mearns et al., 2012; Giorgi, 2019), and to try to understand their simulation biases as much as possible. Towards this end, NARCCAP used NCEP-DOE Reanalysis-2 (R2) data (Kanamitsu et al., 2002) from 1979 to 2004 to drive the RCMs for the simulation of the historical climate of North America. By comparing all regional models within NARCCAP using various metrics, Mearns et al. (2012) provided a baseline evaluation indicating that all models can simulate some aspects of the North American climate reasonably well for the historical period. However, significant differences exist among the models that highlight uncertainties in modeling regional climate processes. To improve the understanding of the errors in the regional climate models, more analyses are needed.

Previous studies have evaluated the NARCCAP RCM simulations for different geographic regions and on different aspects of simulation. Gutowski et al. (2010) found that for coastal California, the models well replicate the frequency and magnitude of extreme monthly precipitation (top 10% of monthly precipitation), and the associated circulation anomaly in the cold half of the year for the period 1982–1999. The models well reproduce the interannual variability of extreme monthly precipitation . For the upper Mississippi River basin, Kawazoe and Gutowski (2013) found that all models generally reproduce the precipitation intensity spectra seen in observations well, with a small tendency toward producing overly strong precipitation at high-intensity thresholds. Wang et al. (2009) evaluated the precipitation climatology of the intermountain region of the Western United States between the Cascade-Sierra range and the Rocky Mountains and found systematic biases with six regional climate models in the NARCCAP. The simulated winter precipitation is too large and the simulated annual cycles are too strong. Leung and Qian (2009) pointed out that during the cold season, the WRF-member simulation in NARCCAP realistically captured the amount and spatial distribution of mean precipitation intensity, extreme precipitation (95th percentile), and the precipitation/temperature anomalies of all the atmospheric river events between 1980–1999 in the topographically diverse western U.S.

For the Central United States, the broad expanse of flat land between the Rocky Mountains and the Mississippi River depends on summer rainfall for its extensive agricultural land use. Thus, the processes contributing to precipitation (Carbone and Tuttle, 2008; Weckwerth and Romatschke, 2019; Trier et al., 2020) and the question of how well numerical models simulate precipitation in the past and predict possible changes in the future have attracted great research interest (Gutowski et al., 2010; Harding and Snyder, 2014). Precipitation across this region is difficult to accurately simulate when using global climate models (GCM) with coarse resolutions (Klein et al., 2006; Harding et al., 2013).

Dynamically downscaling the GCM outputs by using high-resolution RCMs can reduce the simulation bias (Dickinson et al., 1989; Liang et al., 2006). However, the RCMs show conspicuous differences in simulating Central U.S. warm-season rainfall. Some of them oversimulate precipitation over the Central U.S. (Bukovsky and Karoly, 2009; Qiao and Liang, 2015; Kawazoe and Gutowski, 2018). Some of the others undersimulate precipitation in this region (Harding et al., 2013; Gao et al., 2017; Tian et al., 2017; Harris and Lin, 2014; Lee et al., 2007a; Kim et al., 2013). Sun et al. (2016) found that the dynamically downscaled simulations they produced at grid spacings of both 4 km and 25 km share a similar low precipitation bias over the Central U.S. The bias appears to be linked to circulation biases in the simulations. Hu et al. (2018) also noticed significant warm-season precipitation and circulation biases in their dynamically downscaled simulations. Spectral nudging was found to help alleviate the precipitation biases by reducing circulation biases. Kawazoe and Gutowski (2018) found that some RCMs undersimulate the intensity of strong widespread precipitation events in the upper Mississippi region and suggested the need for a deeper look into the connection between the large-scale circulation and precipitation. Overall, the skill of RCMs in simulating precipitation over the Central U.S., and the sources of the precipitation biases still require more detailed assessment and analyses. In the NARCCAP, there are similar warm season precipitation biases among most RCM members; that is, a dry bias over the Central U.S., and a wet bias over the Rocky Mountains region and the southeast coast. The dry bias in the Central U.S. in the WRFG member is about the largest among the NARCCAP RCM members (Mearns et al., 2012) and the WRF model is among the most widely used models for weather prediction and regional climate simulations (Tapiador et al., 2020). For these reasons, this paper focuses on the WRFG member of the NARCCAP simulations and attempts to better understand its behaviors in historical simulations. Specifically, we examine the 19-year period from 1986 through 2004, and assess the performance of the WRFG in reproducing the mean behaviors and diurnal variation of wet season precipitation over the Central U.S. (the red box in Fig. 1), part of the entire model domain that covers the conterminous United States and most of Canada. We further investigate the relationship between precipitation biases and circulation simulation biases, in an attempt to better understand the physical causes of the precipitation bias.

The remainder of this paper is arranged as follows. The data sources are described in section 2. In section 3, we

Surface Altitude (m)
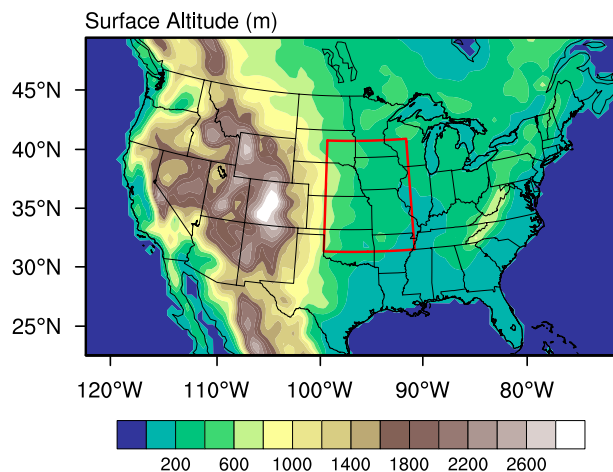
Fig. 1. Terrain elevation (m) of the United States and part of Canada from the WRFG. This is part of the entire model domain which covers the conterminous United States and most of Canada. Our analyses are focused on the Central Great Plains enclosed by the red polygon.

assess how well the WRFG simulates precipitation during the wet season over the Great Plains region of the Central U.S. In section 4, the possible relationship between simulated precipitation, associated circulations, and their biases are discussed. Section 5 summarizes the results and presents conclusions.

2. Data

2.1. *Reference data*

We use the monthly precipitation data from the Parameter-elevation Regressions on the Independent Slopes Model (PRISM) dataset (Daly et al., 1994) as one of the precipitation reference data. We analyze the data during the period from 1986 to 2004 to be consistent with the WRFG simulation. The PRISM monthly mean precipitation dataset (available at http://prism.oregonstate.edu) covering the contiguous U.S. (CONUS) starting in January 1895 is produced by gathering climate observations from a wide range of monitoring networks and through the application of sophisticated quality control measures. We use it in this study because of its high spatial resolution (4-km grid spacing), the use of a sophisticated elevation correction scheme, and inclusion of data from around 8000 stations. More important is its long period of data coverage; the dataset has been used in previous studies evaluating the performance of RCMs (e.g., Hu et al., 2018).

The 4-km NCEP Stage IV precipitation dataset (Lin and Mitchell, 2005) is also used for analysis and comparison (available at https://www.emc.ncep.noaa.gov/mmb/ylin/pcpanl/stage4/). It is mosaicked from regional multi-sensor (radar and gauges) precipitation analyses covering the period from 2002 onward; data up to 2015 are used in this study. The high spatial (4-km grid spacing) and hourly temporal resolutions of the dataset enable an investigation into the diurnal variability of precipitation. The Stage IV product is

currently the only long-running operational product that provides precipitation estimates over the CONUS at high spatial (~4 km) and temporal (hourly) resolutions. Thus, it is used in many studies on precipitation (Nelson et al., 2016). Unfortunately, there is little overlap between the available period of Stage IV data (from 2002 onward) and the WRFG simulation period (1986–2004). Studies have found that the diurnal cycle in summer precipitation has a small year-to-year variation (Dai et al., 1999; Liang et al., 2004), particularly in terms of the diurnal phase. Due to the lack of high spatial and temporal resolution precipitation data set over the WRFG simulation period, we will use the Stage IV data in the 2002-2015 period as a substitution, assuming this aspect, especially the diurnal phase, of precipitation over the central U.S. is similar between the two periods. When the Stage IV data are used for comparison, less emphasis should be placed on precipitation intensity because of possible year-to-year variability.

The NCEP North American Regional Reanalysis (NARR; Mesinger et al., 2006) is a regional, atmospheric reanalysis over North America (available at https://www.esrl.noaa.gov/psd/data/gridded/data.narr.html) that is used to evaluate the WRFG-simulated atmospheric fields including air temperature, wind, moisture, and geopotential height. The NARR dataset covers the years from 1979 through the present. The then-operational NCEP Eta Model with 32-km horizontal grid spacing and 45 layers was used in conjunction with the Regional Data Assimilation System (RDAS) to assimilate precipitation along with other observations. The improvements in the model and data assimilation systems resulted in a dataset with a better accuracy of temperature, winds, and precipitation analyses compared to the NCEP-DOE Global Reanalysis 2 (Mesinger et al., 2006). We use the NARR data, available 8 times daily on 29 vertical levels from 1986 to 2004, to evaluate the WRFG-simulated atmospheric states. We note that the ERA5 (Lavers et al., 2022) global reanalysis dataset is available at hourly intervals but the reanalysis does not assimilate rain-guage precipiation data.

2.2. *WRFG RCM simulation output*

As mentioned earlier, the RCM simulation evaluated in this study is the NARCCAP member using the WRF model with a Grell-Devenyi cumulus parameterization scheme (Mearns et al., 2009). The WRF modeling system is community supported and is widely used throughout the world for a variety of weather and climate applications (Tapiador et al., 2020). However, the WRFG member in NARCCAP has about the largest simulation bias in the region of our research interest which deems a detailed investigation necessary. The WRF model is a fully compressible, non-hydrostatic model with terrain-following, mass-based vertical coordinates and contains a large collection of physical parameterization schemes that can be used to build regional climate simulation systems (Skamarock et al., 2005). In NARCCAP, a WRF member named WRFP was initially run by the Pacific Northwest National Lab (PNNL) using the Kain-Fritsch cumu-

lus parameterization scheme. It was later superseded by a new run that used the Grell-Devenyi cumulus scheme that improved the reproduction of temperature and precipitation, which constitutes the WRFG member that is examined in this study.

For the NARCCAP, the WRF was run at a 50-km horizontal grid spacing with 35 vertical levels over a domain covering the CONUS and most of Canada. Other model physics include the Grell-Devenyi cumulus scheme, the WRF single-moment 5-category (WSM5) microphysics scheme, CAM3 shortwave and longwave radiation scheme, Yonsei University (YSU) planetary boundary layer scheme, and the NOAH land surface model. The full name of this run is WRFG-NCEP, where NCEP indicates the use of NCEP global reanalysis for the initial and lateral boundary forcing. The full length of the simulation spans 1979 to 2004. For this study we examine the 19-year period from 1986 to 2004, which avoids the spin-up period and is still long enough for statistical evaluation (given our focus on the mean behaviors of precipitation simulation and its diurnal variation). Considering that the WRF has many options for physics parameterizations, strictly speaking, our evaluation in this paper is only valid for the particular configurations used. However, some of the behaviors may be common to other physics options or even other models.

3. Assessment of wet season precipitation simulated by the WRFG in the Central U.S.

The climate in the Central U.S. has strong seasonal variability. In this region, more than half of the total annual precipitation occurs during the wet season, which includes late spring and early summer (Wallace, 1975; Higgins et al., 1997; Mearns et al., 2012). In light of this, we assess the simulated precipitation in May, June, and July. To reduce the differences in precipitation intensity purely because of grid resolution difference, we re-grid the ~4 km PRISM and Stage IV precipitation data to the ~50 km WRFG grid by using the NCL ESMF_regrid function with the "conserve" interpolation option. This method tries to preserve the integral value of the interpolated fields and is therefore a preferred choice for mapping high-resolution precipitation to a lower-resolution grid. As seen in Fig. 2a, the average daily mean precipitation intensity in the PRISM data in May is larger than 2 mm d^{-1} in the Central U.S. with the highest intensity of more than 4.5 mm d^{-1} located in the bordering regions of Oklahoma-Kansas and Arkansas-Missouri. May and June are similar in the precipitation distribution pattern but are different in intensity. In June, the rainfall maximum is ~4 mm d^{-1}, weaker than in May (Fig. 2b). In July (Fig. 2c), the rainfall maximum is located at the northeast of Kansas, exceeding ~4 mm d^{-1} over only a small area. In May and June, regions with 3 mm d^{-1} average precipitation extend to the Gulf coast, but in July, these regions move northward as far as northeastern Oklahoma.

In comparison, the WRFG-simulated precipitation is much weaker in all three months (Figs. 2d–f). The WRFG model can roughly reproduce the principal precipitation distribution characteristics over CONUS, that is, large amounts of rainfall in the central and eastern parts of CONUS and little rainfall in the western part of the country from May to July. However, it significantly underestimates the daily mean precipitation intensity in regions of the Gulf of Mexico coast in May (Fig. 2d) and the entire Central U.S. in July (Fig. 2f).

In May (Fig. 2d), daily mean precipitation amounts of over 3 mm d^{-1} are mostly captured over the eastern half of CONUS, but the intensity does not reach 4 mm d^{-1}, even though the observed maximum is more than 4.5 mm d^{-1} (Fig. 2a). The western edge of heavier precipitation also deviates to the east by about 2° longitude or about 200 km (Fig. 2d), and the precipitation within a zone of about 200 km width along the gulf coast is also too weak. The general pattern and intensity of precipitation on the western half of CONUS agree better with observations (Figs. 2a, d).

In June, the simulated dry bias is more significant; it misses all heavy precipitation over 4.5 mm d^{-1} along the Gulf Coast and significantly underpredicts precipitation west of the Mississippi River, especially over the Central and Southern Great Plains (Fig. 2e). In July, the dry bias is even more severe. Nowhere over the Central U.S. does the daily mean precipitation exceed 2.6 mm d^{-1} (Fig. 2f); over the Northern Plains it is about half of the observed amount. Over Central Oklahoma, a minimum of less than 1.1 mm d^{-1} is simulated while the observed amount is around 2.2 mm d^{-1}. The warm season simulation dry bias is consistent with earlier area-averaged precipitation assessments over a similar region in the Central U.S. (Mearns et al., 2012; Kawazoe and Gutowski, 2018).

The diurnal variations of mean precipitation intensity averaged over the Central U.S. within the red polygon in Fig. 1 are shown in Fig. 3 for the Stage IV data for 2002–2015 (solid lines) and the WRFG simulation for 1986–2004 (dashed line) for May, June, and July. The mean precipitation intensities in Stage IV data are obtained by averaging the hourly accumulated precipitation over the previous three hours to the times labeled in the figure. The precipitation intensity in the WRFG is given as the average of instantaneous rainfall rates over the previous three hours. Here, as mentioned earlier, we assume the general stationarity of the precipitation propagation characteristics and diurnal cycles over the past few decades, which is supported by earlier studies.

The general oscillations of diurnal variations in precipitation are reasonably captured in the WRFG simulation, agreeing with previous studies that examined very heavy precipitation events in a similar region (Kawazoe and Gutowski, 2018). However, the amounts and amplitudes are mostly smaller than the observed values, with the relative errors being the smallest in May and the largest in July (Fig. 3) within the region of focus. The peaks of precipitation intensity in the Stage IV data appear at midnight in May and at 3 am local time in June and July while in the model simulation,
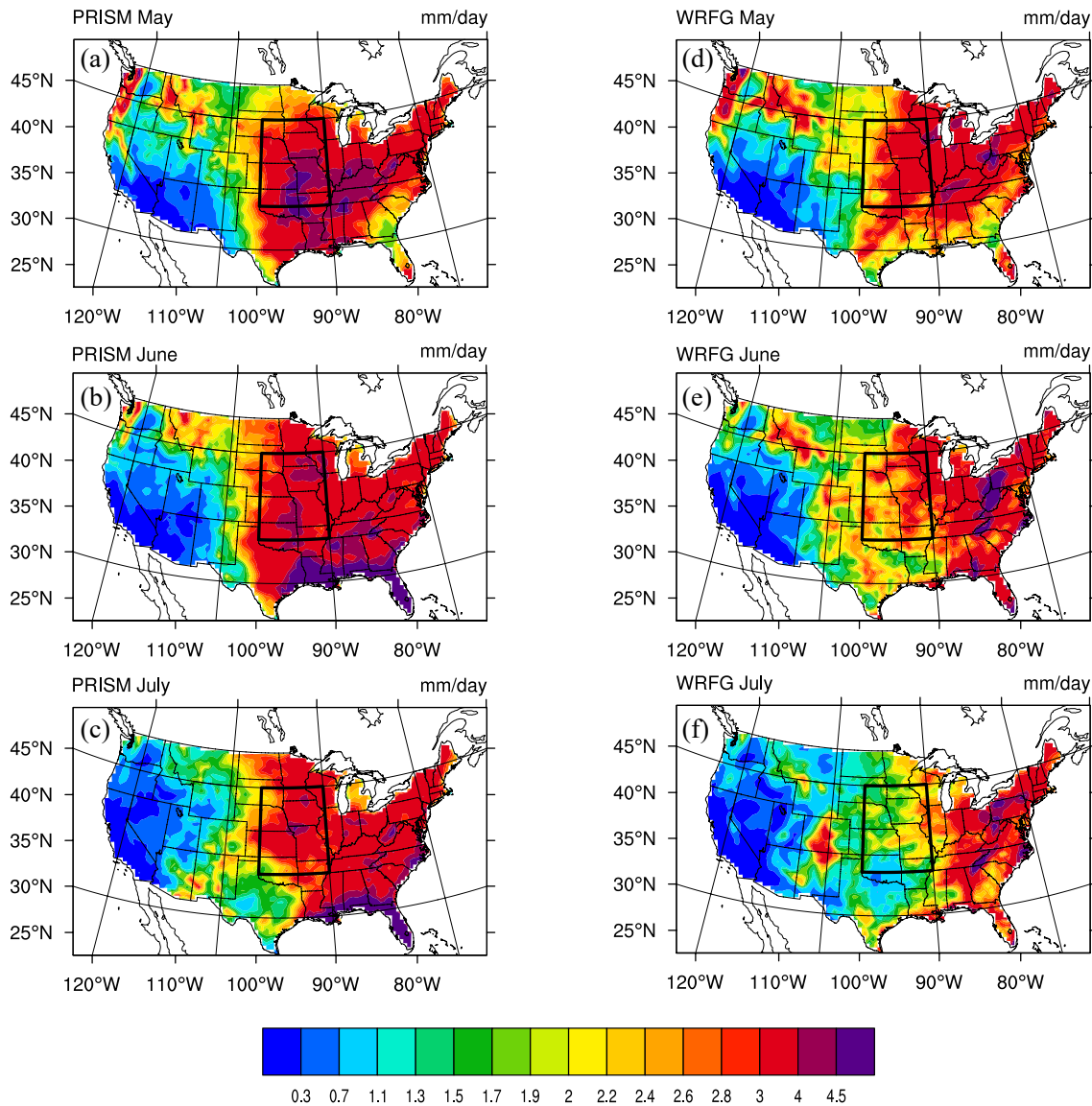
Fig. 2. Spatial distribution of daily mean precipitation intensity averaged over 1986–2004 in PRISM (a) May; (b). June; (c) July, and in the WRFG simulation (d) May; (e) June; (f) July (units: mm d^{-1}).

they all appear at midnight. A pronounced minimum appears at local noon when the intensity is mostly less than half of the peak. The diurnal variation of precipitation patterns for May, June, and July are similar, but the amplitudes of oscillation are different. For May and June, the maximum is about 5 mm d^{-1} while the minimum value is between 2.4 and 2.6 mm d^{-1} in the observations. For July, the variation is between 1.9 and 3.7 mm d^{-1}. These results are consistent with previous studies (e.g., Riley et al., 1987; Wallace, 1975; Higgins et al., 1997; Dai et al., 1999; Carbone et al., 2002; Liang et al., 2004; Tian et al., 2005; Lee et al., 2007a), which reveals that the summer precipitation over the Central U.S. has unique diurnal variations. Nocturnal precipitation accounts for the vast majority of total warm-season precipitation in this region (Higgins et al., 1997; Jiang et al., 2006; Chen et al., 2009).

　　The model-simulated maximum precipitation intensity

in May is about 1 mm d^{-1} smaller than that in the Stage IV data. In July, the simulated value is ~2 mm d^{-1}, about half of the observed value of 3.8 mm d^{-1} in the early morning. Also the observed peak occurs at 3 am, while the simulated amount at midnight is slightly higher. In May and June, both the absolute and relative errors at noon time are relatively small, but those at the midnight peak are much larger. In July, the errors are large for both day and night times. The above results are consistent with the monthly mean precipitation intensity comparisons with PRISM data as presented in Fig. 2, supporting the precipitation stationarity assumption. Overall, the above results also suggest that the primary deficiency of the model in simulating the wet season precipitation over the Central Plains is attributed to its lack of skill in simulating nocturnal precipitation. Since the largest error occurs in July, we will focus the rest of this paper on July and will pay particular attention to nighttime precipitation, to gain an
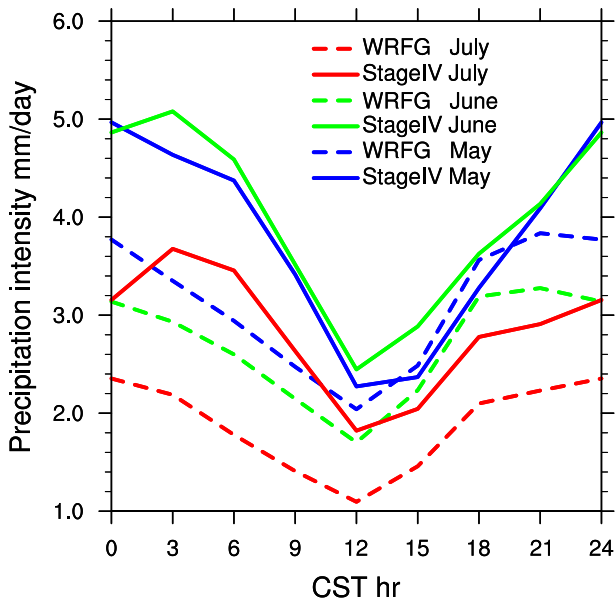
Fig. 3. Diurnal variations of mean precipitation intensity (units: mm d⁻¹) averaged over the Central Great Plains (35°–45°N, 90°–100°W) in the Stage IV dataset (solid line) and in WFRG simulation (dashed line) for May (Blue), June (Green), and July (Red). The mean precipitation intensities are obtained by averaging hourly accumulated precipitation over the previous three hours to the times labeled in the figure.

understanding regarding the nature and causes of such an error.

4. Physical processes associated with the dry bias in the Central U.S.

The nocturnal precipitation maximum over the Central Plains has been attributed to the eastward propagation of convective systems initiated in the afternoon over the Rocky Mountain regions that arrive at the Central Plains at night (e.g., Jiang et al., 2006; Carbone and Tuttle, 2008; Geerts et al., 2017; Weckwerth and Romatschke, 2019), and to locally initiated mesoscale convective systems by the nocturnal low-level jet (Bleeker and Andre, 1951; Blackadar, 1957; Hering and Borden, 1962; Pitchford and London, 1962; Geerts et al., 2017). In the next two sections, we will examine how well the WRFG simulates the eastward propagation of precipitation systems and the synoptic and mesoscale circulations that can affect local forcing to convective systems at night.

4.1. Eastward propagation of convective systems from the Rocky Mountains

The 3-hourly Stage IV precipitation averaged over 2002–2015 is shown in Fig. 4. It is seen that in the afternoon (between 1200 and 1500 CST, CST=UTC−6 hours, Fig. 4h), convective systems are clearly evident over the Rocky Mountain regions of Colorado and New Mexico. Such convection should be due to daytime heating of the elevated terrain. Over the next few hours (between 1500 and 2100 CST,

Figs. 4a, b), the main precipitation zone shifts eastward, located in eastern Colorado between 1800 and 2100 CST, and over the eastern Colorado and New Mexico Borders by 0000 CST (Fig. 4c). Based on a 12-year climatology, Carbone and Tuttle (2008) found that propagating precipitation episodes, i.e., upstream precipitating systems propagating into the region, contributed 60% of the summer rainfall to the Central United States. Weckwerth and Romatschke (2019) examined cases that occurred during the Plains Elevated Convection At Night (PECAN) field campaign (Geerts et al., 2017), and found that 70% of the Great Plains precipitation was caused by episodes that formed outside of the PECAN domain (centered over Kansas) and propagated into the region. Mountain-initiated storms formed primarily in the afternoon and the surviving ones propagated eastward, grew upscale, and contributed 27% to the total precipitation in the plains (Weckwerth and Romatschke, 2019). The fact that the precipitation zone shifts continuously eastward with time as shown in Fig. 4 suggests that the propagation of convection storms initiated over the Rocky Mountains into the Central Plains while growing upscale is responsible for at least part of the nighttime precipitation over the Plains, and this is even more evident when examining hourly precipitation (not shown).

By 0300 CST, most of the precipitation is over the central part of the Great Plains (Fig. 4d), and by early morning it is mostly located over the eastern borders of Oklahoma, Kansas, and into Iowa and areas further to the north (Fig. 4e). Between 00 and 0600 CST, precipitation is mainly found over the central part of the Central Great Plains. Such precipitation is believed to be linked to the Great Plains nocturnal low-level jet, whose northern terminus is located in the Central Great Plains during this period (e.g., Weckwerth and Romatschke, 2019; Trier et al., 2020), and the merger of the systems propagating into the region with locally-initiated precipitation would also play a role, as documented in Weckwerth and Romatschke (2019). At 0300 CST (Fig. 4d), the precipitation budget box used in Fig. 3 (see Fig. 1) is filled with both convective systems that have propagated into the region and systems that initiated locally; this would explain the precipitation peak at 0300 CST in the region seen in Fig. 3.

Over the three hours following 0600 CST, the main precipitation zone continues to shift eastward, to a north-south axis through Central Arkansas by 0900 CST. Such a shift should be related to the eastward propagation of convective systems (e.g., Carbone and Tuttle, 2008). The systems in Central Plains weaken significantly between 0600 and 0900 CST, and are mostly dissipated after 0900 CST (Fig. 4g). At 1200 CST (noon), the precipitation over the Central U.S. is indeed at a minimum (Fig. 4g) while by mid-afternoon (Fig. 4h), new convection has developed, over the Rockies, the eastern part of U.S. and over parts of the Central Plains (Fig. 4h). Most of the heavy precipitation along the Gulf Coast seen in the PRISM data (Fig. 2) is clearly from afternoon convection (Fig. 4h). The propagation of convective sys-
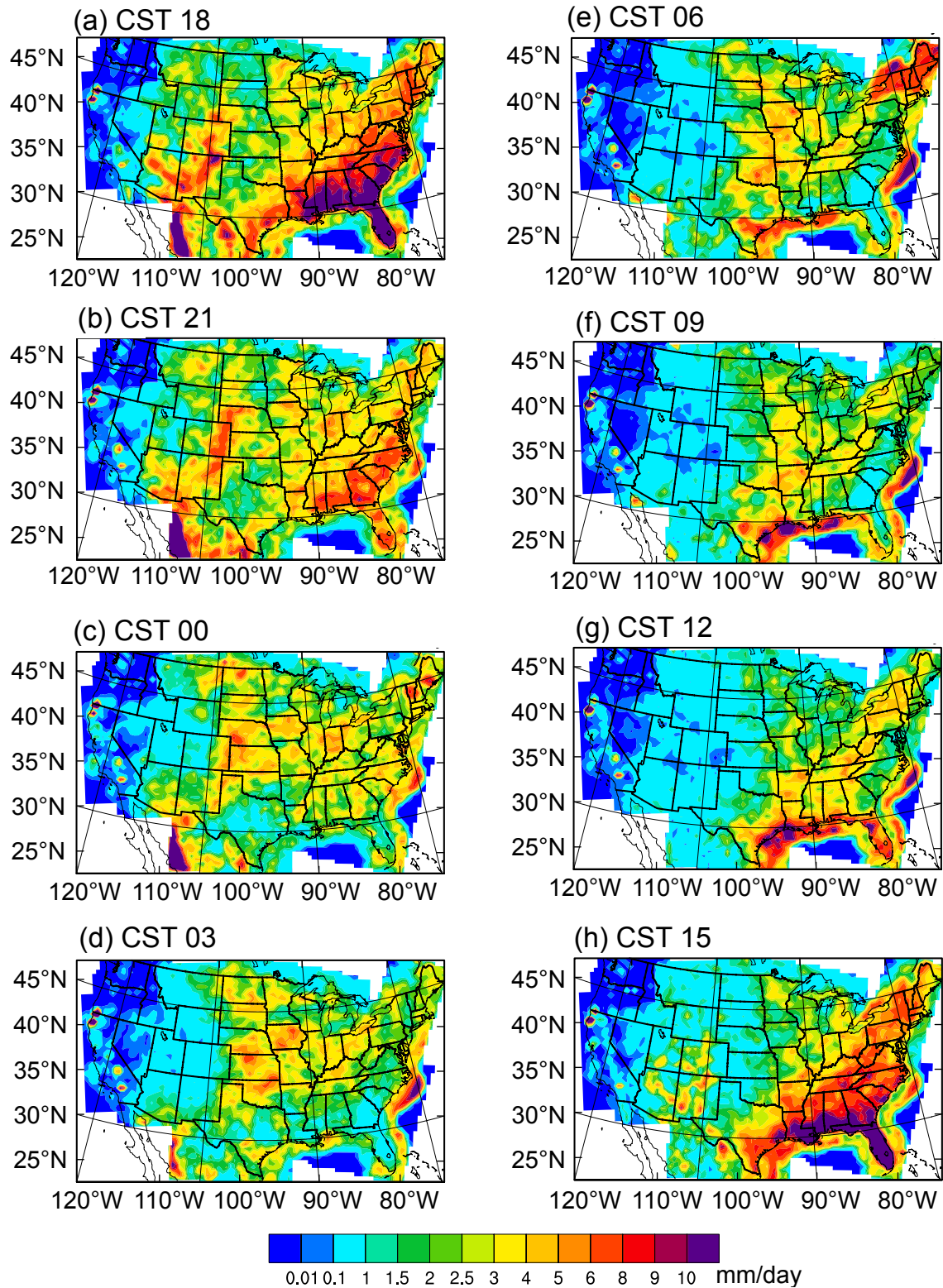
Fig. 4. Spatial distributions of precipitation intensity (units: mm d^{-1}) in July averaged over 2002−2015 for Stage IV data for the central standard times indicated in the panels. The precipitation intensities are obtained by averaging hourly accumulated precipitation over the previous three hours to the times labeled in the figures.

tems across the Central Plains overnight discussed above agrees with previous studies that some of the convective storms initiated over the Rockies in the afternoon can propagate eastward and become organized, creating coherent struc-

tures in precipitation Hovmöller diagrams (Carbone et al., 2002; Liang et al., 2004; Jiang et al., 2006). The eastward propagation of organized convective systems is indeed an important contributor to the nocturnal precipitation over the

Great Plains (Jiang et al., 2006; Weckwerth and Romatschke, 2019). Thus, whether the model can reasonably reproduce the eastward propagation of convective systems initiated over the Rockies would affect its performance in simulating the timing, distribution, and intensity of nighttime pre-

cipitation in the Central U.S.

The WRFG-simulated 3-hourly precipitation intensities averaged over the 1986–2004 simulation period, are plotted in Fig. 5. The difference in the averaging periods is due to the difference in data availability, as discussed earlier. It
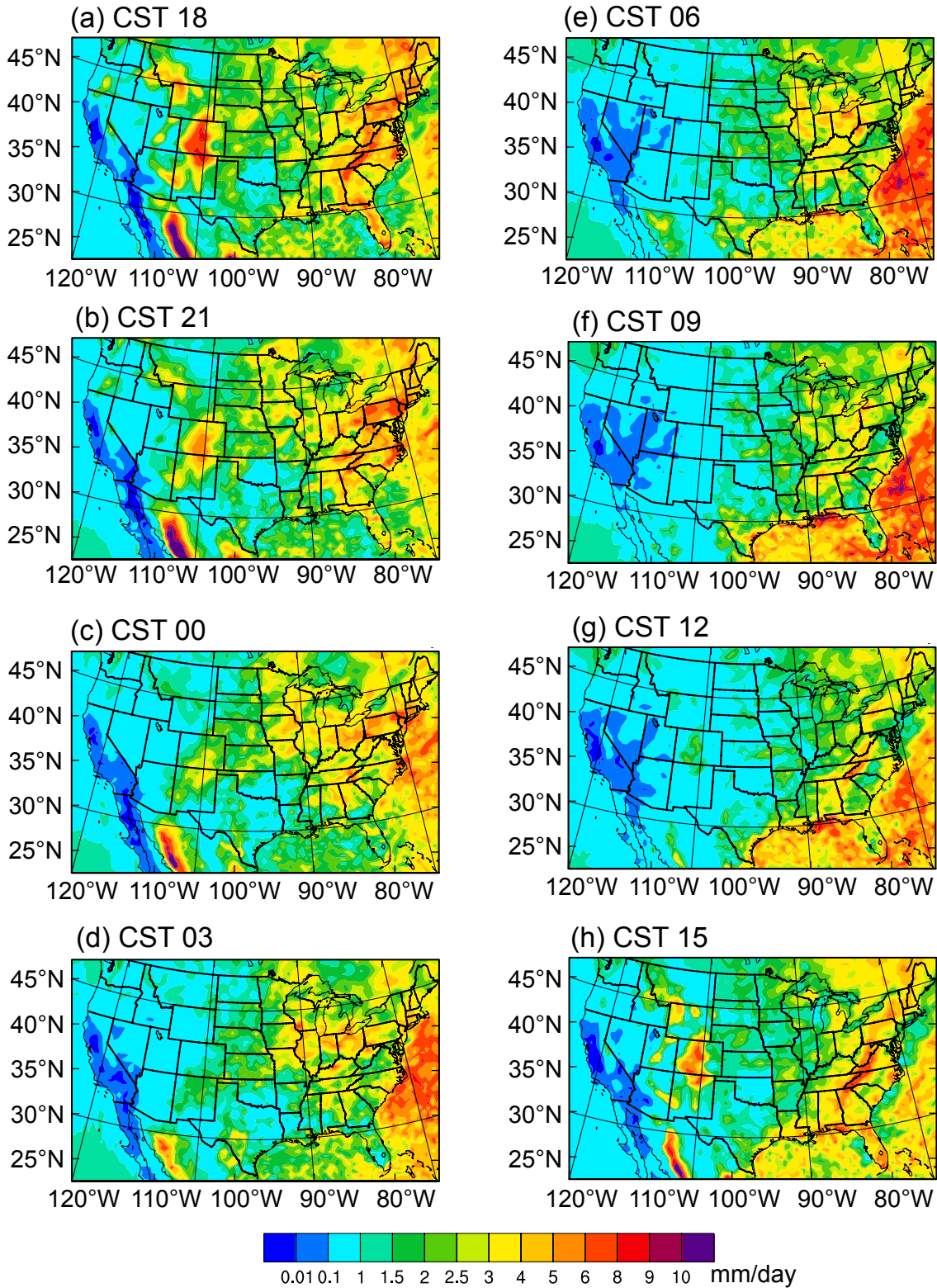
Fig. 5. Spatial distribution of precipitation intensity in July averaged over 1986–2004 in the WRFG simulation (units: mm d^{-1}).

should be pointed out that due to this difference, the comparison between the precipitation intensities among the two datasets should be viewed with caution, due to possible year-to-year variability in precipitation amounts. For example, certain years can be wetter than other years. The emphasis of the comparisons in Figs. 3–6 should be placed on the diurnal temporal variations and spatial propagation, and less so on intensity. For these comparisons, we are effectively assuming the general stationarity of the precipitation propagation and diurnal variation characteristics over the past few decades, which is supported by earlier studies indicating that the diurnal cycle in summer precipitation has small year-to-year variability (Dai et al., 1999; Liang et al., 2004).

Figure 5 shows that there are clear pattern differences between the simulation and Stage IV data. In the afternoon (Fig. 5h), precipitation develops over the Colorado and New Mexico mountains, due to convection from thermal forcing. However, such convection fails to organize into long-lived MCSs and dissipates before moving much farther eastward onto the Plains. (Figs. 5a–d). Over the Great Plains, there is scattered precipitation from the afternoon to the next early morning (Figs. 5a–f) that appears to be strongest around midnight (Fig. 5c). The weaker simulated precipitation over the North-central Great Plains at midnight (Fig. 5c) roughly corresponds to the locally developed precipitation in the observations (Fig. 4c). The precipitation over the Great Plains weakens after midnight, mostly dissipating by the following noon (Figs. 5d–f).

The difference in the propagation characteristics is further illustrated by Hovmöller diagrams of precipitation averaged over the 35°–45°N latitude band (the southern and northern boundaries of the red budget box in Fig. 1) and normalized by daily average precipitation (Fig. 6). In the Stage IV data (Fig. 6a), precipitation first occurs in the afternoon after 1400 CST over the Rocky Mountains west of 105°W, then starts to move eastward from the mountainous region afterward at a speed of about 10° longitude over 12 hours. The most intense precipitation reached 100°W around midnight while the eastern edge had reached 95°W. The precipitation continues to move eastward and reaches 90°W at around 0600 CST at its leading edge (Fig. 6a). The rate of eastward propagation appears to accelerate somewhat between 0300 and 0600 CST; this should be a result of locally developing precipitation after 0300 CST to the east (around 95°W) instead of being all caused by eastward propagation. The precipitation is weakest between 0900 and 1500 CST. Collectively, these results are consistent with the overall diurnal variations of precipitation over the Central Plains as discussed earlier.

Within the WRFG simulation, between the 100°–95°W longitudinal zone, the precipitation maximum is found between 1800 CST and 0000 CST (Fig. 6b), roughly 3 hours earlier than observed, and the propagating precipitation is also displaced eastward by about 5° (Fig. 6a). To the west of 105°W, the afternoon precipitation does not show much sign of eastward propagation and the most intense precipitation remains west of 109°W (Fig. 6b). In fact, between 105°W and 100°W, and from 2100 CST to 0300 CST, there appears to be a precipitation 'trough', suggesting in another way the lack of eastward propagation of precipitation across the region into the Central Plains. The stronger precipitation east of 100°W between 1800 CST and 0000 CST appears to be locally initiated and it does show signs of eastward propagation after formation (Fig. 6b). The above results clearly show that the WRFG fails to reproduce the eastward propagation of convection that develops in the afternoon over the Rockies, that, based on the Stage IV data and other earlier
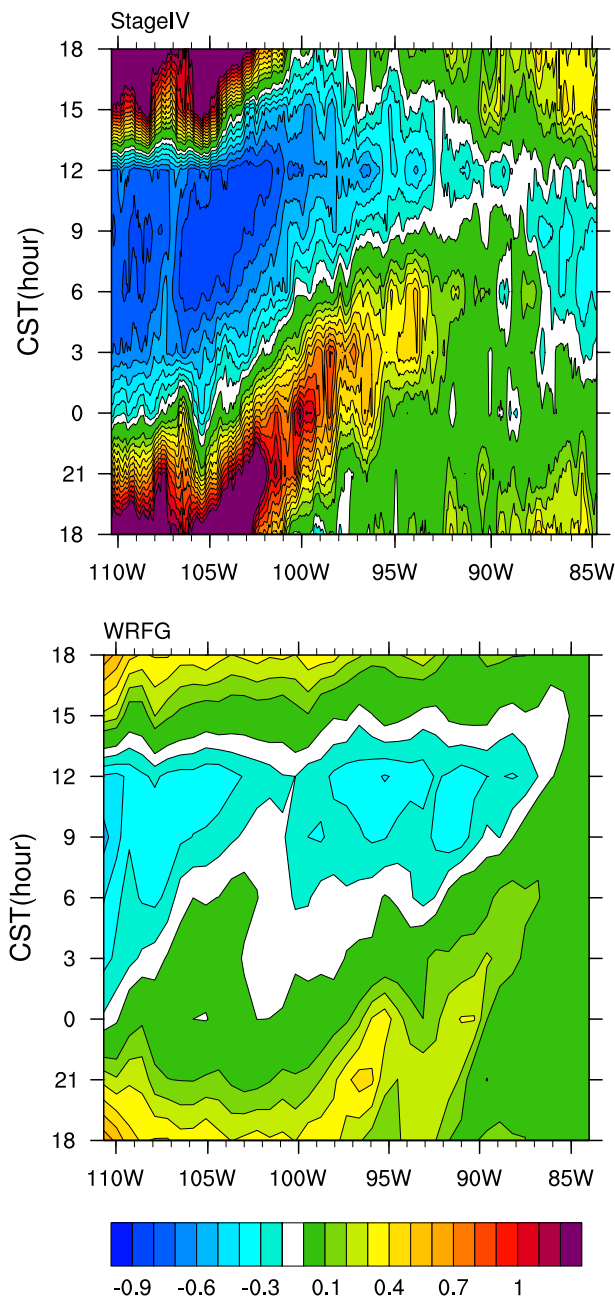
Fig. 6. Hovmöller diagrams of July diurnal precipitation subtracted by and normalized by the daily mean, averaged over the 35°–45°N latitude band, in Stage IV data (top) and precipitation simulated by the WRFG (bottom).

studies, are important contributors to the nighttime and overall precipitation over the Central Plains.

The anomaly in simulating the eastward propagation of convective systems has also been reported in other regional climate simulations (Klein et al., 2006; Lee et al., 2007b; Sun et al., 2016; Hu et al., 2018). The difficulty for models that rely on cumulus parameterizations to produce most convective precipitation has been pointed out in previous research (e.g., Molinari and Dudek, 1992; Weisman et al., 1997; Dai et al., 1999; Gochis et al., 2002; Klein et al., 2006; Brockhaus et al., 2008; Harding et al., 2013). Models run at convection-allowing/resolving resolutions are significantly better at reproducing the propagation of mesoscale convective systems (e.g., Davis et al., 2003; Clark et al., 2009; Lim et al., 2014; Sun et al., 2016; Kwon and Hong, 2017; Hu et al., 2018). Given that many climate simulations will continue to use convection-parameterizing resolutions, especially for global climate models (Gutowski et al., 2020), this problem remains important, especially for regions where precipitation is significantly affected by propagating systems. A reasonable solution has to be found for future regional climate simulations at convection-parameterizing resolutions, concerning water cycles. The defect of the model in simulating the eastward propagation process at least partly contributes to its dry bias in simulating precipitation in the Central U.S..

4.2. *Large-scale atmospheric circulation and environmental conditions*

Mesoscale convective systems (MCSs) most often develop in favorable large-scale environments with adequate water vapor, atmospheric instability, and effective uplift (Houze, 2004; Loriaux et al., 2016). Thus, how well a regional climate model simulates the large-scale environmental conditions that trigger and force convection affects its performance in simulating precipitation. Hence, we evaluate the regional atmospheric circulation and environmental conditions simulated by the WRFG and hope to gain further insights into its precipitation simulation error. Because the main precipitation error occurs in the early morning hours,

in the remainder of this section, we will focus on circulations and other atmospheric conditions in the early morning, in particular at 0600 CST (1200 UTC) when reanalysis data are available.

4.2.1. *Large-scale atmospheric circulation*

Figure 7 shows the 850-hPa geopotential height and horizontal wind field in the early morning at 0600 CST of July averaged over 1986–2004 in the NARR reanalysis data (Fig. 7a) and WRFG simulation (Fig. 7b). The Bermuda High, a semi-permanent, subtropical high pressure in the North Atlantic Ocean off the east coast of North America is closely linked to the regional climate of the central and eastern parts of U.S. (Stahle and Cleaveland, 1992; Henderson and Vega, 1996; Katz et al., 2003; Diem, 2006; Li et al., 2011; Ortegren et al., 2011). Using the 1560 gpm contour at 850 hPa to represent the boundary of the Bermuda High, following Li et al. (2011), it appears narrower in its north-south extent, and its east-west ridge axis is located further north, from the observed ~25°N to a simulated ~31°N in the WRFG. Such a northward displacement implies that there is a stronger easterly and a weaker southerly component in the onshore flow towards Texas from the Gulf of Mexico in the WRFG compared to that in the observation, potentially transporting less moisture from the Gulf into the Central U.S. On the northwest side of the Bermuda High, the southerly flows appear to extend further north in the NARR than in the WRFG, again potentially bringing more moisture and high-instability air into the Central U.S. Apart from these potentially important differences in details, overall, the circulation pattern over CONUS is reproduced reasonably well.

To reveal the relationship between the Great Plains precipitation and the low-level atmospheric circulation, we calculate the correlation coefficient of the July precipitation intensity within the red budget box of Fig. 1 (blue box in Fig. 8) and the 850-hPa geopotential height at individual grid points, and the correlation coefficients between the precipitation intensity and the 850-hPa horizontal wind components (Fig. 8a) using the NARR reanalysis. For the wind components, the two correlation coefficients are plotted in the
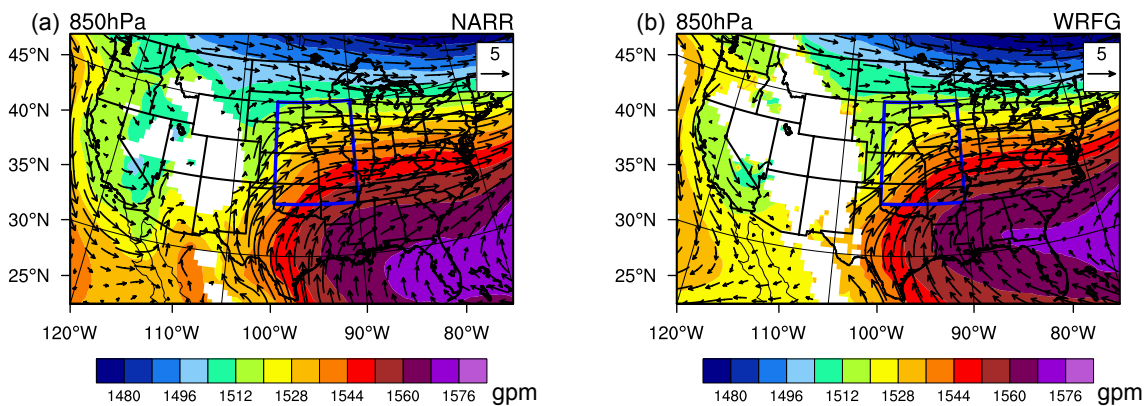
Fig. 7. The 850-hPa geopotential height (shading, units: gpm) and horizontal wind (vector, units: m s^{-1}) at 0600 CST averaged in July over 1986–2004 in the (a) NARR reanalysis and (b)WRFG simulation.
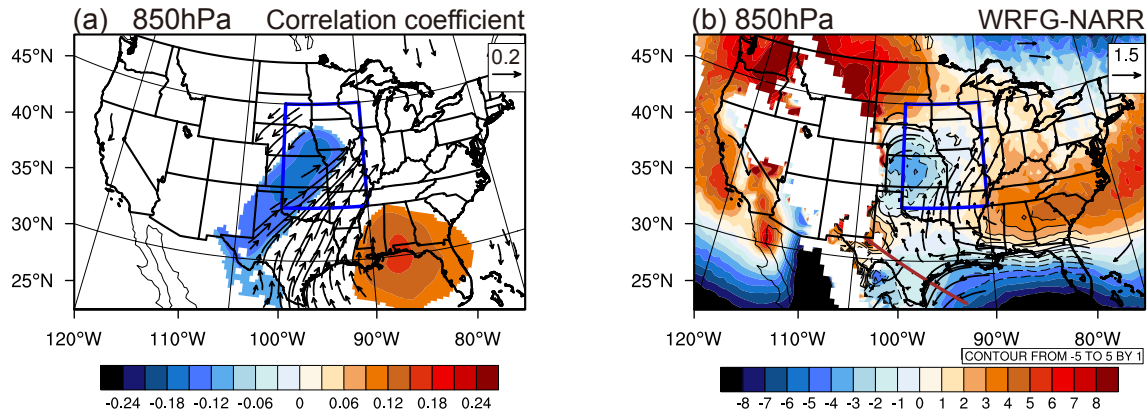
Fig. 8. The correlation coefficient of the overall Great Plains precipitation intensity within the red budget box in Fig. 1 and 850-hPa geopotential height (shading), and the correlation coefficients of 850-hPa zonal and meridional wind components with Great Plains precipitation intensity respectively (vector) that are (a) significant at the 99% confidence level. The correlation statistics are calculated using data at 0600 CST daily in July during the study period. The projection of the vector in the latitudinal direction represents the correlation coefficient of zonal wind speed and precipitation intensity, and the projection of the vector in the meridional direction represents the correlation coefficient of meridional wind speed and precipitation intensity; so that a long northeastward pointing vector denotes large positive correlations with both wind components. Difference fields between the WRFG and NARR (WRFG – NARR) in the 850-hPa geopotential height (shading, unit: gpm) and horizontal wind (vector, m s^{-1}) at 0600 CST in July are averaged over 1986–2004 (b).

form of vectors, so that a long northeastward-pointing vector means large positive correlations with both components. Figure 8 shows that the precipitation intensity within our budget box is negatively correlated to the 850-hPa height in a zone stretching from southwestern Texas through southwestern Iowa, and positively correlated with the 850-hPa height in the coastal regions of the eastern Gulf of Mexico, with a maximum located along the Alabama coast. Such a correlation pattern clearly indicates that the precipitation in our budget region is positively correlated with the geopotential height gradient along the northwestern perimeter of Bermuda High, which is directly linked to the geostrophic wind speed along the perimeter. This is confirmed by the correlation coefficient vectors shown in Fig. 8a. Stronger southwesterly winds at the 850-hPa level between the locations with positive and negative height correlation coefficients enhance precipitation in the Central U.S. The southwesterly winds, making up a synoptic low-level jet (LLJ) at the perimeter of the Bermuda High, transport warm, moist maritime air from the Gulf of Mexico to the Great Plains and the Midwest region and greatly impact the precipitation distribution and intensity over this region (Helfand and Schubert, 1995; Higgins et al., 1997; Zhu and Liang, 2005, 2007; Wang and Chen, 2009). Consequently, errors in predicting such flows would lead to errors in the simulated precipitation simulation in the region.

The difference fields between the WRFG simulation and the NARR reanalysis in 850-hPa geopotential height and winds (Fig. 8b) show a 'horse saddle' pattern, with two high anomaly centers located in Western Texas (likely extending all the way to the Northwestern U.S.) and the Eastern U.S. and two low anomaly centers over Kansas and the Gulf of Mexico. Such a pattern corresponds to too weak subtropical

high over the Gulf, and too high pressure over western Texas—leading to too weak east-west pressure gradient over southern Texas, the path of warm moist air from the Gulf into the Central Great Plains. Related to this pattern, the flows near the southern Texas Gulf coast show a northerly anomaly what would act to reduce onshore moisture transport (Fig. 8b). Further, there is a northerly wind anomaly in Western Texas and a southeasterly wind anomaly in Northeast Texas. These differences are partially the result of an eastward shift of southerly LLJ, possibly leading to less convective storm initiation in the western parts of Texas and Oklahoma. The suggested negative biases in warm moist air transport from the Gulf into Central Great Plains can explain to some extent the dry bias in the WRFG over the Central U.S. Further north, the height anomaly pattern implies the presence of a higher pressure gradient and stronger 850-hPa southerly flows in the WRFG over the southeastern part of our budget box. However, such a flow anomaly appears to have mostly originated from the southeastern coastal regions rather than from the ocean in the Gulf. Also, even if these flows transport more moisture, this moisture transport will mainly contribute to precipitation in the midwest region, outside of our budget box.

Figure 9 shows the vertical cross-sections of mean air temperature and geopotential height at 0600 CST in July, with their horizontal means removed, along the northwest-southeast slope in Texas (denoted as the brown line in Fig. 8b). The topography decreases from West Texas to the coastal region. In the lower levels of the troposphere, there is a warm low-pressure system over the plateau and a cold high-pressure system over the Gulf Coastal Plain. The absorption of solar radiation by the land surface causes it to act as an elevated heat source for the atmosphere. The horizontal
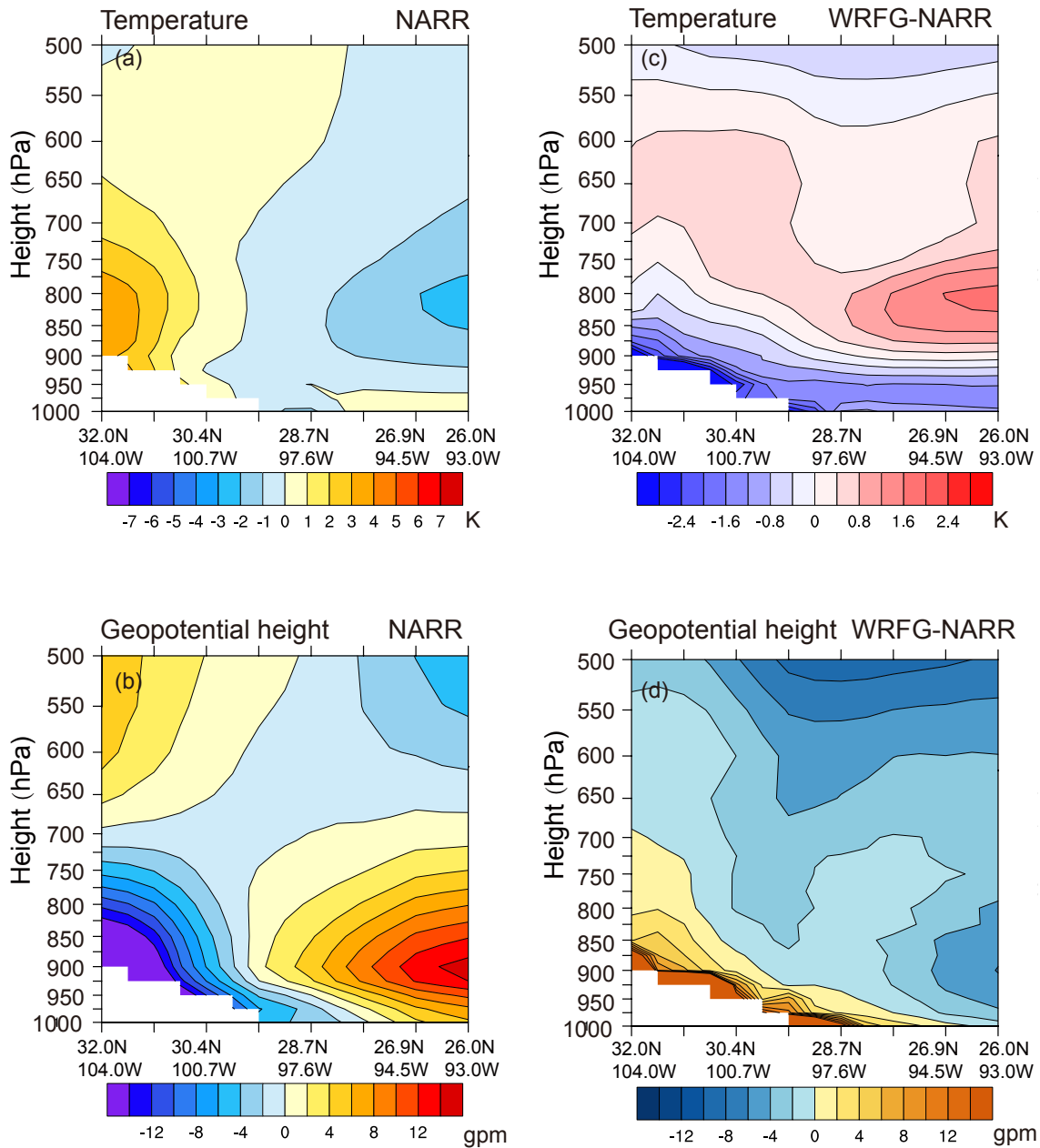
Fig. 9. Vertical cross-section of the (a) NARR air temperature and (b) geopotential height with their horizontal means removed; and (c) air temperature (units: gpm) and (d) geopotential height difference fields between the WRFG and NARR at 0600 CST of July (units: K). The cross-section is along the northwest-southeast slope over southwestern Texas leading to the New Mexico Plateau, as denoted by the brown line in Fig. 8b.

thermal contrast (Fig. 9a) partially leads to the horizontal pressure gradient (by lowering the pressure on the west side, Fig. 9b), and southerly winds over Texas (Fig. 10a) in the lower troposphere in the NARR reanalysis. The difference fields between the WRFG simulation and the NARR reanalysis in Fig. 9c., clearly show a cold temperature bias within about 1 km above the land surface in the simulation. At the 825-hPa level, the along-slope thermal contrast is one-third smaller in the simulation. Correspondingly, the horizontal geopotential height gradient along the slope is about 50% smaller in simulation than in the NARR reanalysis (Fig. 9d). Collectively, the above considerations may constitute one of

the reasons for the simulation bias in the low-level southerly winds (Fig. 10).

In the NARR reanalysis data, the time-averaged southerly LLJ is in the lower troposphere over the sloping terrain from the New Mexico Plateau to the plains in Central and Eastern Texas (Fig. 10a). The climatologically averaged maximum meridional wind speed of the jet is larger than 8 m s^{-1} at the height of about 1 km above the ground. The LLJ can be decomposed into geostrophic and ageostrophic wind components. The geostrophic meridional component is southerly from the surface to the middle troposphere (Fig. 10b). The height of the LLJ is about 875 hPa over the
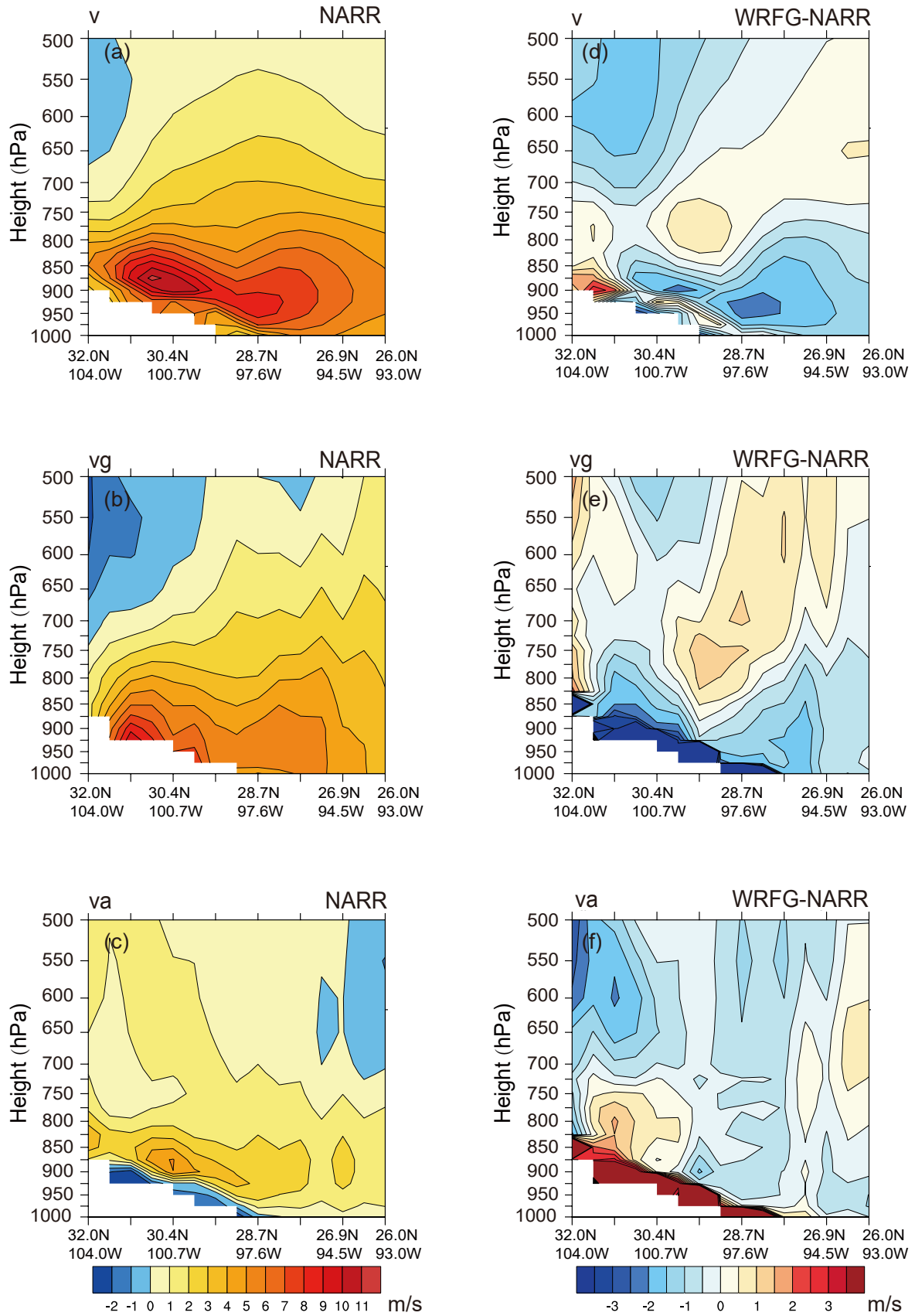
Fig. 10. Vertical cross-section along the brown line in Fig. 8b, of (a) meridional wind, (b) meridional geostrophic wind, and the (c) meridional ageostrophic wind of the mean NARR. The right panels show the corresponding difference fields between the WRFG and NARR at 0600 CST of July (units: m s^{-1}).

plateau and about 925 hPa over the Plains; over these regions, these heights are within the planetary boundary layer. The LLJ reaches peak intensity in the early morning and the boundary layer inertial oscillation is believed to be the primary cause (Blackadar, 1957). The geostrophic meridional wind is about 6 m s^{-1} and the ageostrophic meridional component at the same height is weaker, about 3 m s^{-1}. The difference fields between the WRFG and NARR show that the simulated meridional wind of the LLJ is about 2 m s^{-1} weaker, and the core of LLJ is shifted downward compared to the NARR (Fig. 10d). These results echo and enrich research that reported that the WRFG tends to underestimate the warm season southerly LLJ frequency, speed, and elevation at the rawinsonde locations in the Central Plains (Tang et al., 2016). They further highlighted the need to further examine the differences in the jet formation mechanisms. Our research indicates that the aforementioned simulated precipitation bias can be at least partially attributed to the weaker southerly geostrophic wind component (Fig. 10e). At the level of the LLJ core, there is a clear northerly anomaly in the geostrophic winds (Fig. 10e), which is likely related to the error in land surface processes in the WRFG that affects the east-west geopotential height gradient. The simulated southerly ageostrophic wind at the level of the LLJ core is weaker (Fig. 10f). The downward shift of the LLJ core is related to the near-ground southerly anomaly of the ageostrophic wind. This suggests possible error sources in boundary layer parameterization, because of the key role of the boundary layer inertial oscillation in producing the boundary layer nocturnal LLJ (Blackadar, 1957; Xue et al., 2018; Huang et al., 2022).

4.2.2.   *Environmental conditions*

The previously discussed LLJ simulation biases can cause biases in moisture transport toward the Central Plains

leading to errors in the simulated precipitation over the Central U.S. The NARR reanalysis (Fig. 11a) clearly shows a water vapor transport channel over the east-west sloping terrain, transporting moisture northward. The moisture transport channel is roughly located at the level of the boundary layer LLJ, which is about 1 km above the slope. The maximum meridional moisture transport is at ~875 hPa over the plateau and at ~950 hPa over the Plains. In the WRFG, the low-level water vapor transported through this cross-section is about 25% less than in the NARR based on the difference field (Fig. 11b). Considering that a significant part of the convective systems in Central U.S. has their updraft source at low levels (Weckwerth et al., 2004), we use the vertically integrated moisture flux convergence from the surface to 700 hPa to determine the favorable locations for the development of moist convection (Banacos and Schultz, 2005). In the NARR reanalysis, the water vapor from the Gulf of Mexico travels through Texas before converging in the downstream regions over Oklahoma, Arkansas, Missouri, Kansas, and southern Iowa in July (Fig. 12a). While in the WRFG, the water vapor convergence in Oklahoma and Kansas is smaller and there is little moisture convergence in Iowa (Fig. 12b). This can potentially contribute to the dry bias in the simulation.

The atmospheric circulation transports not only moisture but also energy from subtropical regions to the higher latitudes by the LLJ. The poleward moving flow carries high-energy and high-entropy air at low levels, which can rise under appropriate vertical lifting in the mid-latitudes, thereby affecting the generation and maintenance of mesoscale convective systems (Pauluis et al., 2008). The northward energy transport by the warm moist air can be approximately expressed as moist enthalpy transport. The moist enthalpy is defined by:
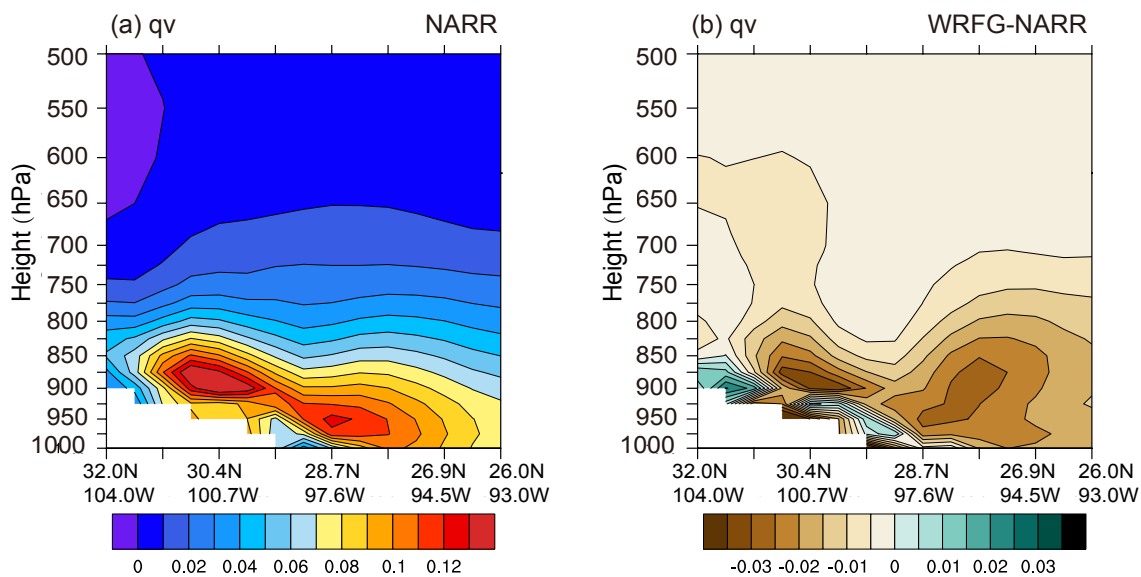
Fig. 11. Vertical cross-section of meridional moisture flux (units: m kg kg^{-1} s^{-1}) in the (a) NARR, and (b) WRFG – NARR (The cross-section is along the northwest-southeast slope which is denoted by the brown line in Fig. 8b). The plotted are mean fields of 0600 CST in July.
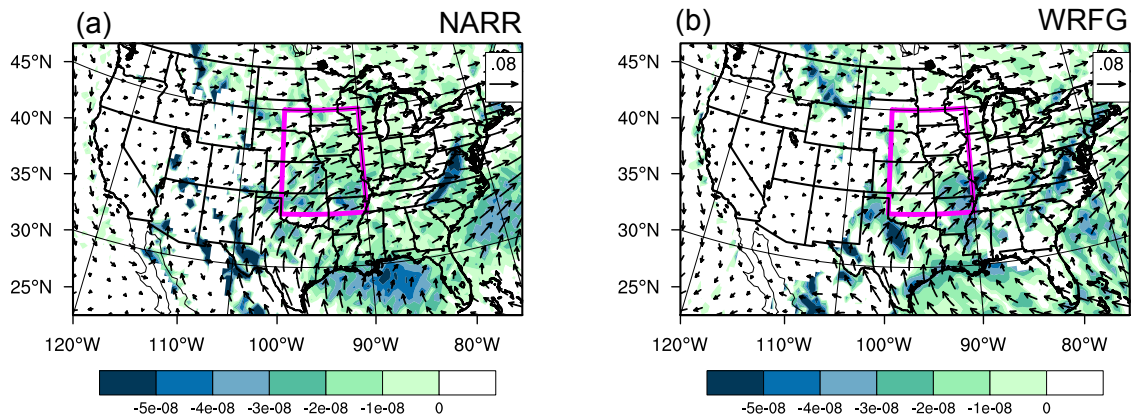
Fig. 12. Horizontal moisture flux (vector, units: m kg kg^{-1} s^{-1}) and moisture flux divergence (shading, units: kg kg^{-1} s^{-1}) vertically integrated from the 1000 hPa to 700 hPa in the (a) NARR and (b) WRFG. The mean fields of 0600 CST in July are plotted.

$$H = C_p T + L q_v \,, \tag{1}$$

where C_p is the heat capacity of the dry air at constant pressure, T is the temperature, q_v is the specific humidity, and L is the latent heat of vaporization of liquid water. It follows that the northward moist enthalpy transport flux is:

$$vH = v C_p T + v L q_v \,, \tag{2}$$

where v is the meridional wind component. The northward moist enthalpy transport consists of the meridional sensible heat flux and latent heat flux. The NARR reanalysis data show that the maximum sensible heat is transported northward in the lower troposphere, within which the core of sensible heat flux is located at about 1 km above the slope ground surface, apparently because of the boundary layer LLJ (Fig. 13a). Its maximum center is mainly located west of 100°W. In the WRFG, less sensible heat is transported northward (Fig. 13b), and the maximum center is shifted eastward to ~97°W at the ~925 hPa level. In the NARR reanalysis, the northward latent heat flux has almost the identical location and pattern in the vertical cross-section as the sensible heat flux, apparently due to the LLJ again (Fig. 13c). The simulated northward latent heat flux is also weaker and its maximum location is shifted eastward (Fig. 13d). In general, lower amounts of latent heat and sensible heat are transported northward from the Gulf to the Great Plains in the WRFG simulation than in NARR and the maximum transport channel is shifted eastward by several degrees. Less energy transport implies weaker convection and less precipitation in the simulation.

The lifting of air parcels to their level of free convection is a necessary ingredient for deep moist convection (Houze, 2004; Loriaux et al., 2016). In the Central U.S., the forcing needed to provide low-level lift often comes from boundary layer flow convergence (Fig. 14a). In the reanalysis data, there is general convergence at 850 hPa over the Central U.S., with the strongest convergence found in Oklahoma, Kansas, Arkansas, and Missouri within our budget box.

Such low-level convergence in the early morning hours is mainly due to the deceleration of southerly LLJ in the region, and is further aided by enhancement to the LLJ at night due to boundary layer inertial oscillations (Blackadar, 1957). The super-geostrophic nocturnal LLJ is more effective at creating horizontal flow convergence than the synoptic scale LLJ that is mostly geostrophic because the latter is nearly non-divergent (Xue et al., 2018). In the WRFG simulation, the low-level convergence is weaker in the southwestern part of our budget box while the low-level flows in the northern part are mostly divergent (Fig. 14b). While the weaker low-level convergence and upper-level divergence could be a result of weaker precipitation in the WRFG, the former is more likely the cause of weaker locally initiated convection, because nighttime precipitation over the Central Plains is known to be forced by boundary layer convergence related to the nocturnal LLJ.

5. Summary and conclusions

In this study, the PRISM and Stage IV precipitation data, and the NARR reanalysis data set are used to assess the performance of an RCM WRFG simulation of the Central U.S. wet-season precipitation from 1986 to 2004. The WRFG uses the WRF model with a 50-km grid spacing with the Grell-Devenyi cumulus parameterization scheme; it is a member of the North American Regional Climate Change Assessment Program (NARCCAP). This member is chosen for detailed evaluation because the WRF model is the most widely used community model for both weather prediction and regional climate simulations. It has about the largest precipitation simulation bias among the NARCCAP members over the Central U.S. Great Plains. Previous studies have evaluated the NARCCAP simulations over other parts of the U.S. but less so over the Central Great Plains. In this region, significant biases are found with the precipitation simulation of the WRFG. We evaluate regional atmospheric circulation and environmental conditions biased in the WRFG simulation to help elucidate the possible origins of its precipita-
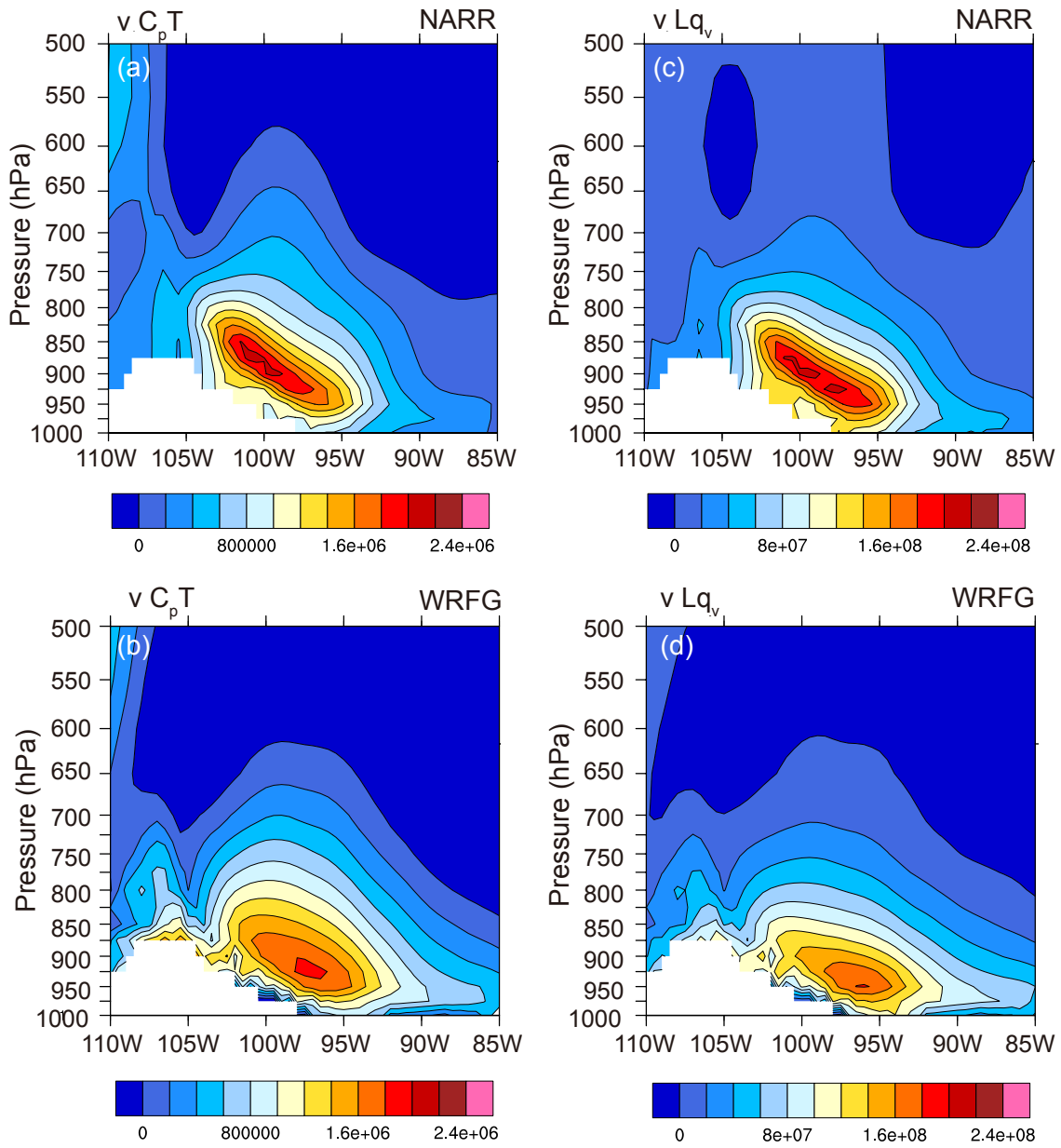
Fig. 13. Meridional sensible heat flux (units: m J s^{-1} kg^{-1}) averaged over the 30°–42.5°N latitudinal band for the (a) NARR and (b) WRFG, and the meridional latent heat flux (units: m J s^{-1} g^{-1}) averaged over the 30°–42.5°N latitudinal band for the (c) NARR and (d) WRFG.
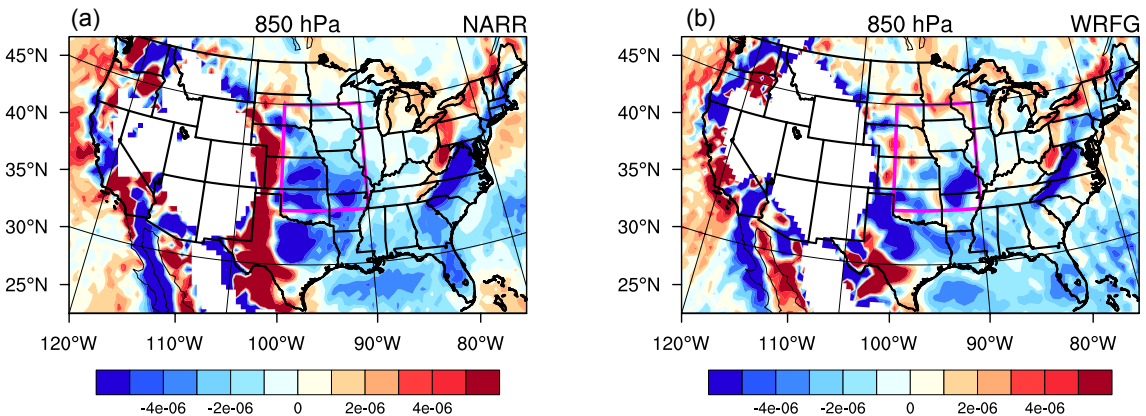
Fig. 14. Horizontal divergence at 850 hPa in the (a) NARR, (b) WRFG (units: s^{-1}).

tion simulation error sources.

Results show that the WRFG model can generally reproduce the distribution characteristics of late spring to early summer precipitation, but it underestimates precipitation intensity in the Central Great Plains. The primary deficiency of the model in simulating wet-season precipitation over the Central Great Plains is linked to its lack of skill in simulating nocturnal precipitation. One reason is that WRFG fails to reproduce the eastward propagation of convective systems that develop in the afternoon over the Rockies, which are important contributors to the nighttime and overall precipitation over the Central Plains. This deficiency is commonly known to simulations at resolutions that require cumulus parameterization, and improvement to the cumulus parameterization scheme is clearly needed for future regional climate simulations. An alternative is to perform the simulations at convection-allowing resolutions so that cumulus parameterization is no longer necessary, although the precipitation simulation biases may not be completely eliminated (Sun et al., 2016).

Locally developed nocturnal convection and precipitation are equally important for the Central Plains region, and such precipitation is usually forced by boundary layer convergence at the northern terminus of nocturnal boundary layer LLJ, and the LLJ also plays an important role in transporting warm and moist air from the Gulf of Mexico into the Great Plains. Hence, the model's ability to accurately simulate the intensity and location of the LLJ, as well as other related environmental conditions, is another important factor to examine.

In the WRFG simulation, it is found that, on average, the subtropical high over the Gulf is too weak and while the simulated pressure over western Texas is too high, leading to horizontal pressure gradient that is too weak over southern Texas, which is on the path of warm moist air moving from the Gulf into the Central Great Plains. Related to this pressure pattern, the flows near the southern Texas Gulf coast show a northerly anomaly (the difference of simulated values from reanalysis) that would act to reduce onshore moisture transport. Further, there is also a northerly anomaly in West Texas. The simulated early morning LLJ is also weaker and is displaced to the east by several degrees of longitude. These differences lead to negative biases regarding warm moist air, and hence the moist energy transport from the Gulf of Mexico into the Central Great Plains.

Low-level convergence in the Central Great Plains is found to be weaker in the simulation, consistent with the weaker LLJ. The weak biases in the northward synoptic-scale flows on the periphery of the subtropical high, and the weak biases in the nocturnal LLJ from the Southern and Central Great Plains in the WRFG simulation are other important reasons that contribute to the simulated nocturnal precipitation over the Central Great Plains being too weak. Reducing model error in these aspects is important; higher horizontal and vertical resolutions and improved parameterization schemes, including the planetary boundary layer scheme,

are likely needed. Spectral nudging can be used to force large-scale circulations towards the reanalysis but does not solve the bias problem for future regional climate simulation if the global climate model simulation that provides the lateral boundary forcing also has the error (Hu et al., 2018). Clearly, further refinement to the WRFG RCM configurations is needed for it to be effectively used for reliable future climate dynamic downscaling, or post-processing, and calibration is needed based on past climate simulation results. Other recent studies indicate that the lack of proper representation of topography, land-surface processes, and groundwater-atmosphere interactions in models can lead to losses in soil moisture flux that reduce MCS genesis. Such errors can also be possible causes for the Central Great Plains dry bias (e.g., Prein et al., 2020; Barlage et al., 2021). The deficiencies regarding a realistic representation of cloud microphysical processes and MCS kinematic properties are also among the possible causes of error (Wang et al., 2022). To fully understand the reasons for the biases, more numerical experiments are needed, together with a detailed diagnostic analysis of the simulation results.

REFERENCES

Banacos, P. C., and D. M. Schultz, 2005: The use of moisture flux convergence in forecasting convective initiation: Historical and operational perspectives. *Wea. Forecasting*, **20**, 351−366, https://doi.org/10.1175/WAF858.1.

Barlage, M., F. Chen, R. Rasmussen, Z. Zhang, and G. Miguez-Macho, 2021: The importance of scale-dependent groundwater processes in land-atmosphere interactions over the central United States. *Geophys. Res. Lett.*, **48**, e2020GL092171. https://doi.org/10.1029/2020GL092171.

Blackadar, A. K., 1957: Boundary layer wind maxima and their significance for the growth of nocturnal inversions. *Bull. Amer. Meteor. Soc.*, **38**, 283−290, https://doi.org/10.1175/1520-0477-38.5.283.

Bleeker, W., and M. J. Andre, 1951: On the diurnal variation of precipitation, particularly over central U.S.A., and its relation to large-scale orographic circulation systems. *Quart. J. Roy. Meteor. Soc.*, **77**, 260−271, https://doi.org/10.1002/qj.49707733211.

Brockhaus, P., D. Lüthi, and C. Schär, 2008: Aspects of the diurnal cycle in a regional climate model. *Meteor. Z.*, **17**, 433−443, https://doi.org/10.1127/0941-2948/2008/0316.

Bukovsky, M. S., and D. J. Karoly, 2009: Precipitation simulations

using WRF as a nested regional climate model. *J. Appl. Meteorol. Climatol.*, **48**, 2152–2159, https://doi.org/10.1175/2009JAMC2186.1.

Carbone, R. E., and J. D. Tuttle, 2008: Rainfall occurrence in the U.S. warm season: The diurnal cycle. *J. Climate*, **21**, 4132–4146, https://doi.org/10.1175/2008JCLI2275.1.

Carbone, R. E., J. D. Tuttle, D. A. Ahijevych, and S. B. Trier, 2002: Inferences of predictability associated with warm season precipitation episodes. *J. Atmos. Sci.*, **59**, 2033–2056, https://doi.org/10.1175/1520-0469(2002)059<2033:IOPAWW>2.0.CO;2.

Caya, D., and R. Laprise, 1999: A semi-implicit semi-lagrangian regional climate model: The Canadian RCM. *Mon. Wea. Rev.*, **127**, 341–362, https://doi.org/10.1175/1520-0493(1999)127<0341:ASISLR>2.0.CO;2.

Chen, H. M., T. J. Zhou, R. C. Yu, and J. Li, 2009: Summer rain fall duration and its diurnal cycle over the US Great Plains. *International Journal of Climatology*, **29**, 1515–1519, https://doi.org/10.1002/joc.1806.

Clark, A. J., W. A. Gallus, M. Xue, and F. Y. Kong, 2009: A comparison of precipitation forecast skill between small convection-allowing and large convection-parameterizing ensembles. *Wea. Forecasting*, **24**, 1121–1140, https://doi.org/10.1175/2009WAF2222222.1.

Dai, A. G., F. Giorgi, and K. E. Trenberth, 1999: Observed and model-simulated diurnal cycles of precipitation over the contiguous United States. *J. Geophys. Res.: Atmos.*, **104**, 6377–6402, https://doi.org/10.1029/98JD02720.

Daly, C., R. P. Neilson, and D. L. Phillips, 1994: A statistical-topographic model for mapping climatological precipitation over mountainous terrain. *J. Appl. Meteorol. Climatol.*, **33**, 140–158, https://doi.org/10.1175/1520-0450(1994)033<0140:ASTMFM>2.0.CO;2.

Davis, C. A., K. W. Manning, R. E. Carbone, S. B. Trier, and J. D. Tuttle, 2003: Coherence of warm-season continental rainfall in numerical weather prediction models. *Mon. Wea. Rev.*, **131**, 2667–2679, https://doi.org/10.1175/1520-0493(2003)131<2667:COWCRI>2.0.CO;2.

Dickinson, R. E., R. M. Errico, F. Giorgi, and G. T. Bates, 1989: A regional climate model for the western United States. *Climatic Change*, **15**, 383–422, https://doi.org/10.1007/BF00240465.

Diem, J. E., 2006: Synoptic-scale controls of summer precipitation in the southeastern United States. *J. Climate*, **19**, 613–621, https://doi.org/10.1175/JCLI3645.1.

Gao, Y., L. R. Leung, C. Zhao, and S. Hagos, 2017: Sensitivity of U.S. summer precipitation to model resolution and convective parameterizations across gray zone resolutions. *J. Geophys. Res.: Atmos.*, **122**, 2714–2733, https://doi.org/10.1002/2016JD025896.

Geerts, B., and Coauthors, 2017: The 2015 plains elevated convection at night field project. *Bull. Amer. Meteor. Soc.*, **98**, 767–786, https://doi.org/10.1175/BAMS-D-15-00257.1.

Giorgi, F., 2019: Thirty years of regional climate modeling: Where are we and where are we going next?. *J. Geophys. Res.: Atmos.*, **124**(11), 5696–5723, https://doi.org/74210.1029/2018JD030094.

Giorgi, F., M. R. Marinucci, and G. T. Bates, 1993a: Development of a second-generation regional climate model (RegCM2). Part I: Boundary-layer and radiative transfer processes. *Mon. Wea. Rev.*, **121**, 2794–2813, https://doi.org/10.1175/1520-0493(1993)121<2794:DOASGR>2.0.CO;2.

Giorgi, F., M. R. Marinucci, G. T. Bates, and G. De Canio, 1993b: Development of a second-generation regional climate model (RegCM2). Part II: Convective processes and assimilation of lateral boundary conditions. *Mon. Wea. Rev.*, **121**, 2814–2832, https://doi.org/10.1175/1520-0493(1993)121<2814:DOASGR>2.0.CO;2.

Gochis, D. J., W. J. Shuttleworth, and Z. L. Yang, 2002: Sensitivity of the modeled North American monsoon regional climate to convective parameterization. *Mon. Wea. Rev.*, **130**, 1282–1298, https://doi.org/10.1175/1520-0493(2002)130<1282:SOTMNA>2.0.CO;2.

Grell, G. A., and D. Dévényi, 2002: A generalized approach to parameterizing convection combining ensemble and data assimilation techniques. *Geophys. Res. Lett.*, **29**, 38-1–38-4, https://doi.org/10.1029/2002GL015311.

Grell, G. A., J. Dudhia, and D. Stauffer, 1994: A description of the fifth-generation Penn State/NCAR mesoscale model (MM5). No. NCAR/TN-398+STR, https://doi.org/10.5065/D60Z716B.

Gutowski, W. J., and Coauthors, 2010: Regional extreme monthly precipitation simulated by NARCCAP RCMs. *Journal of Hydrometeorology*, **11**, 1373–1379, https://doi.org/10.1175/2010JHM1297.1.

Gutowski, W. J., and Coauthors, 2020: The ongoing need for high-resolution regional climate models: Process understanding and stakeholder information. *Bull. Amer. Meteor. Soc.*, **101**, E664–E683, https://doi.org/10.1175/BAMS-D-19-0113.1.

Harding, K. J., and P. K. Snyder, 2014: Examining future changes in the character of Central U.S. warm-season precipitation using dynamical downscaling. *J. Geophys. Res.: Atmos.*, **119**, 13 116–13 136, https://doi.org/doi:10.1002/2014JD022575.

Harding, K. J., P. K. Snyder, and S. Liess, 2013: Use of dynamical downscaling to improve the simulation of Central U.S. warm season precipitation in CMIP5 models. *J. Geophys. Res.: Atmos.*, **118**, 12 522–12 536, https://doi.org/10.1002/2013JD019994.

Harris, L. M., and S. J. Lin, 2014: Global-to-regional nested grid climate simulations in the GFDL high resolution atmospheric model. *J. Climate*, **27**, 4890–4910, https://doi.org/10.1175/JCLI-D-13-00596.1.

Helfand, H. M., and S. D. Schubert, 1995: Climatology of the simulated great plains low-level jet and its contribution to the continental moisture budget of the United States. *J. Climate*, **8**, 784–806, https://doi.org/10.1175/1520-0442(1995)008<0784:COTSGP>2.0.CO;2.

Henderson, K. G., and A. J. Vega, 1996: Regional precipitation variability in the southern United States. *Physical Geography*, **17**, 93–112, https://doi.org/10.1080/02723646.1996.10642576.

Hering, W. S., and T. R. Borden, 1962: Diurnal variations in the summer wind field over the central United States. *J. Atmos. Sci.*, **19**, 81–86, https://doi.org/10.1175/1520-0469(1962)019<0081:dvitsw>2.0.co;2.

Higgins, R. W., Y. Yao, E. S. Yarosh, J. E. Janowiak, and K. C. Mo, 1997: Influence of the Great Plains low-level jet on summertime precipitation and moisture transport over the central United States. *J. Climate*, **10**, 481–507, https://doi.org/10.1175/1520-0442(1997)010<0481:IOTGPL>2.0.CO;2.

Houze, R. A. Jr., 2004: Mesoscale convective systems. *Rev. Geophys.*, **42**, RG4003, https://doi.org/. https://doi.org/10.1029/

2004RG000150.

Hu, X.-M., M. Xue, R. A. McPherson, E. Martin, D. H. Rosendahl, and L. Qiao, 2018: Precipitation dynamical downscaling over the Great Plains. *Journal of Advances in Modeling Earth Systems*, **10**, 421−447, https://doi.org/10.1002/2017MS001154.

Huang, X. G., C. Zhang, J. F. Fei, X. P. Cheng, J. L. Ding, and H. S. Liu, 2022: Uplift mechanism of coastal extremely persistent heavy rainfall (EPHR): The key role of low-level jets and ageostrophic winds in the boundary layer. *Geophys. Res. Lett.*, **49**, e2021GL096029. https://doi.org/10.1029/2021GL096029.

Jiang, X. N., N. C. Lau, and S. A. Klein, 2006: Role of eastward propagating convection systems in the diurnal cycle and seasonal mean of summertime rainfall over the U.S. Great Plains. *Geophys. Res. Lett.*, **33**, L19809. https://doi.org/10.1029/2006GL027022.

Juang, H. M. H., S. Y. Hong, and M. Kanamitsu, 1997: The NCEP regional spectral model: An update. *Bull. Amer. Meteor. Soc.*, **78**, 2125−2144, https://doi.org/10.1175/1520-0477(1997)078<2125:TNRSMA>2.0.CO;2.

Kanamitsu, M., W. Ebisuzaki, J. Woollen, S.-K. Yang, J. J. Hnilo, M. Fiorino, and G. L. Potter, 2002: NCEP–DOE AMIP-II Reanalysis (R-2). *Bull. Amer. Meteor. Soc.*, **83**, 1631−1644, https://doi.org/10.1175/BAMS-83-11-1631.

Katz, R. W., M. B. Parlange, and C. Tebaldi, 2003: Stochastic modeling of the effects of large-scale circulation on daily weather in the southeastern U.S. *Climatic Change*, **60**, 189−216, https://doi.org/10.1023/A:1026054330406.

Kawazoe, S., and W. J. Gutowski Jr., 2013: Regional, very heavy daily precipitation in NARCCAP simulations. *Journal of Hydrometeorolohy*, **14**, 1212−1227, https://doi.org/10.1175/JHM-D-12-068.1.

Kawazoe, S., and W. J. Gutowski Jr., 2018: Evaluation of regional very heavy precipitation events during the summer season using NARCCAP contemporary simulations. *International Journal of Climatology*, **38**, s832−s846, https://doi.org/10.1002/joc.5412.

Kim, J., and Coauthors, 2013: Evaluation of the surface climatology over the conterminous united states in the north american regional climate change assessment program hindcast experiment using a regional climate model evaluation system. *J. Climate*, **26**, 5698−5715, https://doi.org/10.1175/JCLI-D-12-00452.1.

Klein, S. A., X. N. Jiang, J. Boyle, S. Malyshev, and S. C. Xie, 2006: Diagnosis of the summertime warm and dry bias over the U.S. Southern Great Plains in the GFDL climate model using a weather forecasting approach. *Geophys. Res. Lett.*, **33**, L18805. https://doi.org/10.1029/2006GL027567.

Kwon, Y. C., and S. Y. Hong, 2017: A mass-flux cumulus parameterization scheme across gray-zone resolutions. *Mon. Wea. Rev.*, **145**, 583−598, https://doi.org/10.1175/MWR-D-16-0034.1.

Lavers, D. A., A. Simmons, F. Vamborg, and M. J. Rodwell, 2022: An evaluation of ERA5 precipitation for climate monitoring. *Quart. J. Roy. Meteor. Soc.*, **148**, 3152−3165, https://doi.org/10.1002/qj.4351.

Lee, M.-I., and Coauthors, 2007a: An analysis of the warm-weason diurnal cycle over the Continental United States and Northern Mexico in general circulation models. *Journal of Hydrometeorology*, **8**, 344−366, https://doi.org/10.1175/JHM581.1.

Lee, M. I., and Coauthors, 2007b: Sensitivity to horizontal resolution in the AGCM simulations of Warm season diurnal cycle of precipitation over the United States and Northern Mexico. *J. Climate*, **20**, 1862−1881, https://doi.org/10.1175/JCLI4090.1.

Leung, L. R., and Y. Qian, 2009: Atmospheric rivers induced heavy precipitation and flooding in the western U.S. simulated by the WRF regional climate model. *Geophys. Res. Lett.*, **36**, L03820. https://doi.org/10.1029/2008GL036445.

Li, W. H., L. F. Li, R. Fu, Y. Deng, and H. Wang, 2011: Changes to the North Atlantic subtropical high and its role in the intensification of summer rainfall variability in the southeastern United States. *J. Climate*, **24**, 1499−1506, https://doi.org/10.1175/2010JCLI3829.1.

Liang, X. Z., L. Li, A. G. Dai, and K. E. Kunkel, 2004: Regional climate model simulation of summer precipitation diurnal cycle over the United States. *Geophys. Res. Lett.*, **31**, L24208. https://doi.org/10.1029/2004GL021054.

Liang, X. Z., J. P. Pan, J. H. Zhu, K. E. Kunkel, J. X. L. Wang, and A. G. Dai, 2006: Regional climate model downscaling of the U.S. summer climate and future change. *J. Geophys. Res.: Atmos.*, **111**, D10108. https://doi.org/10.1029/2005JD006685.

Lim, K. S. S., S. Y. Hong, J. H. Yoon, and J. Han, 2014: Simulation of the summer monsoon rainfall over East Asia using the NCEP GFS cumulus parameterization at different horizontal resolutions. *Wea. Forecasting*, **29**, 1143−1154, https://doi.org/10.1175/WAF-D-13-00143.1.

Lin, Y., and K. E. Mitchell, 2005: The NCEP stage II/IV hourly precipitation analyses: Development and applications. 19th Conf. on Hydrology, American Meteorological Society, San Diego, CA, USA, Paper 1.2. [Available online at https://ams.confex.com/ams/Annual2005/webprogram/Paper83847.html.]

Loriaux, J. M., G. Lenderink, and A. P. Siebesma, 2016: Peak precipitation intensity in relation to atmospheric conditions and large-scale forcing at midlatitudes. *J. Geophys. Res.: Atmos.*, **121**, 5471−5487, https://doi.org/. https://doi.org/10.1002/2015JD024274.

Mearns, L. O., W. Gutowski, R. Jones, R. Leung, S. McGinnis, A. Nunes, and Y. Qian, 2009: A regional climate change assessment program for North America. *Eos, Transsactions American Geophysical Union*, **90**, 311. https://doi.org/10.1029/2009EO360002.

Mearns, L. O., and Coauthors, 2012: The north american regional climate change assessment program: Overview of phase I results. *Bull. Amer. Meteor. Soc.*, **93**, 1337−1362, https://doi.org/10.1175/BAMS-D-11-00223.1.

Mesinger, F., and Coauthors, 2006: North American regional reanalysis. *Bull. Amer. Meteor. Soc.*, **87**, 343−360, https://doi.org/10.1175/BAMS-87-3-343.

Molinari, J., and M. Dudek, 1992: Parameterization of convective precipitation in mesoscale numerical models: A critical review. *Mon. Wea. Rev.*, **120**, 326−344, https://doi.org/10.1175/1520-0493(1992)120<0326:POCPIM>2.0.CO;2.

Nakicenovic, N., and Coauthors, 2000: Special report on emissions scenarios: A special report of working group III of the intergovernmental panel on climate change. Cambridge University Press, Cambridge, 599pp.

Nelson, B. R., O. P. Prat, D.-J. Seo, and E. Habib, 2016: Assessment and implications of NCEP Stage IV quantitative precipitation estimates for product intercomparisons. *Wea. Forecasting*, **31**, 371−394, https://doi.org/10.1175/WAF-D-14-00112.1.

Ortegren, J. T., P. A. Knapp, J. T. Maxwell, W. P. Tyminski, and P. T. Soulé, 2011: Ocean–ttmosphere influences on low-frequency warm-season drought variability in the Gulf Coast and southeastern United States. *J. Appl. Meteorol. Climatol.*, **50**, 1177–1186, https://doi.org/10.1175/2010JAMC2566.1.

Pan, Z., J. H. Christensen, R. W. Arritt, W. J. Gutowski, E. S. Takle, and F. Otieno, 2001: Evaluation of uncertainties in regional climate change simulations. *J. Geophys. Res.: Atmos.*, **106**, 17 735–17 751, https://doi.org/10.1029/2001JD900193.

Pauluis, O., A. Czaja, and R. Korty, 2008: The global atmospheric circulation on moist isentropes. *Science*, **321**, 1075–1078, https://doi.org/10.1126/science.1159649.

Pitchford, K. L., and J. London, 1962: The low-level jet as related to nocturnal thunderstorms over midwest United States. *J. Appl. Meteorol.*, **1**, 43–47, https://doi.org/10.1175/1520-0450(1962)001<0043:TLLJAR>2.0.CO;2.

Pope, V. D., M. L. Gallani, P. R. Rowntree, and R. A. Stratton, 2000: The impact of new physical parametrizations in the Hadley Centre climate model: HadAM3. *Climate Dyn.*, **16**, 123–146, https://doi.org/10.1007/s003820050009.

Prein, A. F., C. H. Liu, K. Ikeda, R. Bullock, R. M. Rasmussen, G. J. Holland, and M. Clark, 2020: Simulating North American mesoscale convective systems with a convection-permitting climate model. *Climate Dyn.*, **55**, 95–110, https://doi.org/10.1007/s00382-017-3993-2.

Qiao, F. X., and X. Z. Liang, 2015: Effects of cumulus parameterizations on predictions of summer flood in the Central United States. *Climate Dyn.*, **45**, 727–744, https://doi.org/10.1007/s00382-014-2301-7.

Riley, G. T., M. G. Landin, and L. F. Bosart, 1987: The diurnal variability of precipitation across the central Rockies and adjacent Great Plains. *Mon. Wea. Rev.*, **115**, 1161–1172, https://doi.org/10.1175/1520-0493(1987)115<1161:TDVOPA>2.0.CO;2.

Skamarock, W. C., J. B. Klemp, J. Dudhia, D. O. Gill, D. M. Barker, W. Wang, and J. G. Powers, 2005: A description of the advanced research WRF Version 2. NCAR/TN-468+STR, University Corporation for Atmospheric Research, http://dx.doi.org/10.5065/D6DZ069T.

Stahle, D. W., and M. K. Cleaveland, 1992: Reconstruction and analysis of spring rainfall over the southeastern U. S. for the past 1000 years. *Bull. Amer. Meteor. Soc.*, **73**, 1947–1961, https://doi.org/10.1175/1520-0477(1992)073<1947:RAAOSR>2.0.CO;2.

Sun, X. G., M. Xue, J. Brotzge, R. A. McPherson, X.-M. Hu, and X.-Q. Yang, 2016: An evaluation of dynamical downscaling of central plains summer precipitation using a WRF-based regional climate model at a convection-permitting 4 km resolution. *J. Geophys. Res.: Atmos.*, **121**, 13 801–13 825, https://doi.org/10.1002/2016JD024796.

Tang, Y., S. Y. Zhong, J. A. Winker, and C. K. Walters, 2016: Evaluation of the southerly low-level jet climatology for the central United States as simulated by NARCCAP regional climate models. *International Journal of Climatology*, **36**, 4338–4357, https://doi.org/10.1002/joc.4636.

Tapiador, F. J., A. Navarro, R. Moreno, J. L. Sánchez, and E. García-Ortega, 2020: Regional climate models: 30 years of dynamical downscaling. *Atmospheric Research*, **235**, 104785. https://doi.org/10.1016/j.atmosres.2019.104785.

Tian, B. J., I. M. Held, N. C. Lau, and B. J. Soden, 2005: Diurnal cycle of summertime deep convection over North America: A satellite perspective. *J. Geophys. Res.: Atmos.*, **110**, D08108. https://doi.org/10.1029/2004JD005275.

Tian, B. J., and Coauthors, 2017: Development of a model performance metric and its application to assess summer precipitation over the U.S. great plains in downscaled climate simulations. *Journal of Hydrometeorology*, **18**, 2781–2799, https://doi.org/10.1175/JHM-D-17-0045.1.

Trier, S. B., S. D. Kehler, and J. Hanesiak, 2020: Observations and simulation of elevated nocturnal convection initiation on 24 June 2015 during PECAN. *Mon. Wea. Rev.*, **148**, 613–635, https://doi.org/10.1175/MWR-D-19-0218.1.

Wallace, J. M., 1975: Diurnal variations in precipitation and thunderstorm frequency over the Conterminous United States. *Mon. Wea. Rev.*, **103**, 406–419, https://doi.org/10.1175/1520-0493(1975)103<0406:DVIPAT>2.0.CO;2.

Wang, S.-Y., and T.-C. Chen, 2009: The late-spring maximum of rainfall over the U.S. Central Plains and the role of the Low-Level Jet. *J. Climate*, **22**, 4696–4709, https://doi.org/10.1175/2009JCLI2719.1.

Wang, S. Y., R. R. Gillies, E. S. Takle, and W. J. Gutowski, 2009: Evaluation of precipitation in the Intermountain Region as simulated by the NARCCAP regional climate models. *Geophys. Res. Lett.*, **36**, L11704. https://doi.org/10.1029/2009GL037930.

Wang, D., A. F. Prein, S. E. Giangrande, A. Ramos-Valle, M. Ge, and M. P. Jensen, 2022: Convective updraft and downdraft characteristics of continental mesoscale convective systems in the model gray zone. *J. Geophys. Res.: Atmos.*, **127**, e2022JD036746. https://doi.org/10.1029/2022JD036746.

Weckwerth, T. M., and U. Romatschke, 2019: Where, when, and why did it rain during PECAN?. *Mon. Wea. Rev.*, **147**, 3557–3573, https://doi.org/10.1175/MWR-D-18-0458.1.

Weckwerth, T. M., and Coauthors, 2004: An overview of the international H_2O Project (IHOP_2002) and some preliminary highlights. *Bull. Amer. Meteor. Soc.*, **85**, 253–278, https://doi.org/10.1175/BAMS-85-2-253.

Weisman, M. L., W. C. Skamarock, and J. B. Klemp, 1997: The resolution dependence of explicitly modeled convective systems. *Mon. Wea. Rev.*, **125**, 527–548, https://doi.org/10.1175/1520-0493(1997)125<0527:TRDOEM>2.0.CO;2.

Xue, M., X. Luo, K. F. Zhu, Z. Q. Sun, and J. F. Fei, 2018: The controlling role of boundary layer inertial oscillations in Meiyu frontal precipitation and its diurnal cycles over China. *J. Geophys. Res.: Atmos.*, **123**, 5090–5115, https://doi.org/10.1029/2018JD028368.

Zhu, J. H., and X.-Z. Liang, 2005: Regional climate model simulation of U.S. soil temperature and moisture during 1982–2002. *J. Geophys. Res.: Atmos.*, **110**, D24110, https://doi.org/10.1029/2005JD006472.

Zhu, J. H., and X.-Z. Liang, 2007: Regional climate model simulations of U.S. precipitation and surface air temperature during 1982–2002: Interannual variation. *J. Climate*, **20**, 218–232, https://doi.org/10.1175/JCLI4129.1.